Graphene based Carbon Monoxide Gas Sensor Operating at Room Temperature

By

Muhammad Hamid

School of Chemical and Materials Engineering

National University of Sciences and Technology

2018

Graphene based Carbon Monoxide Gas Sensor Operating at Room Temperature

Name: Muhammad Hamid

Reg. No: 00000172304

This thesis is submitted as a partial fulfillment of the requirements for the degree of

MS in Chemical Engineering

Supervisor Name: **Dr. Tayyaba Noor**

Co-Supervisor: Dr. Farooq Zafar

School of Chemical and Materials Engineering (SCME)

National University of Sciences and Technology (NUST)

H-12 Islamabad, Pakistan

2018

Dedication

To my Parents, Teachers and siblings

Acknowledgments

All acclaim and eminence be to **"ALLAH"** a definitive maker of this universe, who favored us with the capacity to think and made us anxious to investigate this entire universe. Incalculable greetings upon the Holy Prophet **"HAZRAT MUHAMMAD (PEACE BE UPON HIM)"**: the wellspring of information and blessings for whole humankind.

My sincerest thanks to Principal SCME **Prof. Dr. Arshad Hussain** for being a source of great inspiration and for facilitation of this research work. I offer my sincere thanks to Head of Chemical Engineering department, **Dr. Muhammad Bilal Khan Niazi** for his kind assistance and help.

I am extremely obliged to my supervisor, **Dr. Tayyaba Noor** for her encouragement, supervision, and patience throughout my MS studies and for the guidance and assistance during this project with her immense knowledge. It is her consistent encouragement that empowered me to achieve this.

I am thankful to my Co-supervisor **Dr. Farooq Zafar, Dr. Farhat Huma and Mr. Ijaz Ahmad from NESCOM** for her invaluable help, time, feedbacks and support during this research. Their supervision abetted me in every phase of research work and composing of thesis. This thesis would not have been possible without their support, great patience and invaluable feedback.

I express my thanks to my GEC members **Dr. Abdul Qadeer Malik** and **Dr.Sarah Farrukh** for their valuable time for me. I also express my thanks to **Dr. Sofia Javed** for letting me work in Nano Synthesis Lab and **Dr. Mudassir Iqbal** of SNS for allowing me to using equipment of Chemistry Lab. I additionally put on record, my feeling of appreciation to everyone, who straightforwardly or by implication, helped me to finish this work. My thanks also goes to **Mr. Muhammad Zeeshan, Mr. Khurram Shahzad** and **Mr. Shams** from SCME and Naveed Ahmad from USPCAS-E for their valuable help in lab.

I am highly obligated to my family for their never ending love. Thanks for believing in me, wanting the best for me and inspiring me to follow my dreams. I am grateful of your emotional and financial support. To my friends, **Usman, Sammar, Atif and Zarrar** thank you for your support, advice and encouragement.

Abstract

Graphene has got significant scientific attention because of its special chemical, mechanical and electrical properties. This highly strong two dimensional (2D) material has prospective application in gas sensors. Carbon monoxide gas sensor are very important for human health and safety. Carbon monoxide is highly toxic gas and tough to detect because of its colorless and odorless characteristics. Carbon monoxide can get into human blood through lungs or skin. It moves into the tissues where it binds with oxygen and decrease the amount of oxygen there. This leads to headache, dizziness, confusion and even death at high concentration and longtime exposure. Herein, we report the use of defected Graphene (usually called reduced Graphene Oxide), Nitrogen doped reduced Graphene oxide (N-doped rGO) and composites of reduced Graphene Oxide (rGO) with nanoparticle of metal oxide (Fe_3O_4, CoOOH) and MOFs (ZIF-67, Ni-BDC) for carbon monoxide sensing at ambient conditions. Graphene oxide is prepared by chemical oxidation of graphite and converted into reduce graphene oxide (rGO) by using phenyl hydrazine. Metal Oxide nanoparticles (Fe_3O_4 and CoOOH) and MOFs (ZIF-67 and Ni-BDC) were successfully incorporated in rGO and employed for carbon monoxide sensing. Nitrogen doping in graphene was successfully done by using ammonium nitrate as nitrogen source and tested for carbon monoxide gas sensor. The prepared materials GO, rGO, Fe_3O_4, CoOOH, ZIF-67,Ni-BDC and their composites were characterized by X-ray diffraction pattern, Scanning Electron Microscopy, and FT-IR spectroscopy. Reduced graphene oxide has shown 14 % sensitivity with response time of 120s while nitrogen doped reduced graphene oxide shows 80% response towards 1000ppm of CO with response time of 30s. Among Hybrids, rGO/Fe_3O_4 hybrid has shown no response at room temperature while rGO/CoOOH, rGO/ZIF67 and rGO/Ni-BDC shows 34%, 90% and 38% response towards 1000ppm of CO respectively. ZIF-67 gives highest sensitivity (90%) in 20s for 1000ppm of CO level and is a promising candidate for CO sensing application.

Keywords: Graphene Oxide, Reduced Graphene Oxide, Metal Oxide Nanoparticles, Zeolitic Imidazolate Framework-67 (ZIF-67), Ni-BDC, Solvothermal Synthesis, CO sensor.

Table of Contents

List of Figures

List of Tables

Acronyms List

GO	Graphene Oxide
rGO	Reduced Graphene Oxide
N-doped rGO	Nitrogen doped Reduced Graphene Oxide
MOF	Metal Organic Framework
ZIF	Zeolitic Imidazolate Framework
SEM	Scanning Electron Microscope
XRD	X-ray diffraction
FTIR	Fourier Transform Infrared
DMF	Dimethylformamide
BDC	1,4-benzenedicarboxylate
2D	2 Dimensional
3D	3 Dimensional
RT	Room temperatrue

CHAPTER 1

Introduction

Extensive industrialization and use of different chemicals has increased the emissions of toxic gases and vapors to the environment. Among many toxic gases, CO emission is a threat to human life. [1, 2]. The emission of CO can cause diverse effect on human health. CO can get into human blood through lungs or skin, and move into tissues where it binds with oxygen and decrease the amount of oxygen there, which leads to headache, dizziness, confusion and even death at high concentration. Effect of different concentration of CO on humans is given in table 1.1. For environmental monitoring and protection of human health CO detection is important. [2]

Table 1.1. Effects of different concentration of CO on humans.

Concentration	Exposure Time	Symptoms
35 ppm	Six to Eight Hours	Headache and dizziness
100 ppm	Two to Three Hours	Slight headache
840 ppm	50 Min	Nausea, and convulsions
3,200 ppm	Five to Ten Minutes, 30 Minutes	Dizziness, Headache and Death
6,000 ppm	Two Minutes, 20 Minutes	Headache and dizziness. Convulsions, respiratory arrest, and death
12,800 ppm	Three Minutes.	Death

1.1 Common Sources of Carbon Monoxide and Safety Limits

According to World Health Organization (WHO) [3] some common sources of carbon monoxide are Cigarette Smoke, Gasoline Heaters, Propane-Fueled Equipment (Portable Stoves), House Fires, Wood-Burning Stoves, Solid Waste Disposal, Faulty Furnaces, Internal Combustion Vehicle Exhaust and Warehouse. Tobacco burning is another source of indoor CO generation. Two cigarettes produce 80-190mg of CO in 10min.

1.2 Industrial Emissions of Carbon Monoxide

According to Occupational Safety and Health Administration (OSHA) industries and processes that produce CO are; 1. Steel Production by Blast Furnaces 2.Matels Purifying 3.Coke Producing Reactors 4. Carbon Black Manufacture 5. Oil Refining 6. Coal Mining 7. Boiler Rooms 8. Breweries 9. Metabolism of Dichloromethane Produces Carbon Monoxide 10.Paint Industries [4].

1.3 OSHA standards for Carbon Monoxide exposure

According to OSHA following occupations are usually exposed to CO on daily basis 1. Welder 2. Garage mechanic 3. Firefighter 4. Carbon-black maker 5. Organic chemical synthesizer 6. Metal oxide reducer 7. Longshore worker 8. Diesel engine operator 9. Forklift operator 10. Marine terminal worker 11. Toll booth or tunnel attendant. The permissible exposure limit (OSHA PEL) for above mentioned workers during 8 hour time period, is 50 parts per million (ppm) [4].

For maritime operations, OSHA PEL is also 50ppm for 8 hour period, but if CO concentration increases up to 100ppm the maritime workers should be evacuated from workplace. Workers involved in roll in-roll off RO-RO operations (roll-on roll-off operations) the CO OSHA PEL is 200 ppm. According to World Health Organization (WHO) carbon monoxide exposure limits are given in figure 1

Concentration	Time	Concentration	Time
1000 ppm	15 min	300 ppm	1hr
600 ppm	30 min	100 ppm	8 hr

Figure 1: WHO Limits of CO Exposure

1.4 Few Historic Events of Carbon Monoxide Poisoning

In November 1971, Seattle-King County U.S Washington Health Department detected CO illness in 15 children. The cause of their illness was CO exposure of 305ppm in ice-skating arena. [5] On June 2001 B. Marc reported the cause of six deaths in a house to be linked to CO generated by gasoline-powered generator.[6] In 2008, after Hurricane Ike's landfall, large population was effected by CO poisoning. CO generated from electric generators operating in close rooms. [7] On July 18, 2015 a man from Greystanes died because of carbon monoxide poisoning. CO produced from coal which he was using to heat his closed room [8].

1.5 Solid State Carbon Monoxide detectors

The working principle of this type of gas sensors is the revocable contact of gas molecules with sensing material, this interaction alter the electric resistance of sensor, this change in resistance measured as signal. Solid-state gas sensors can be electro-chemical or chemi-resistive.

An electrochemical sensor is very similar to a fuel cell. Electrochemical sensors comprise of electrodes dipped in the electrolyte (usually sulfuric acid) and connecting wires. The REDOX reaction of carbon monoxide occur on electrodes which produce current and this current is measured as a signal.

Chemi-resistive sensors consist of a thin sensing material which is connected to an integrated circuit. Oxygen chemisorbed on sensing element and increase the resistance of the sensor, as the sensor exposed to target gas change in resistance occurs which measured as the response. Because of simplicity and low cost, focus will be on chemi-resistive sensor. However, the sensing mechanism of chemi-resistive gas sensor is multifaceted and under research. [9].

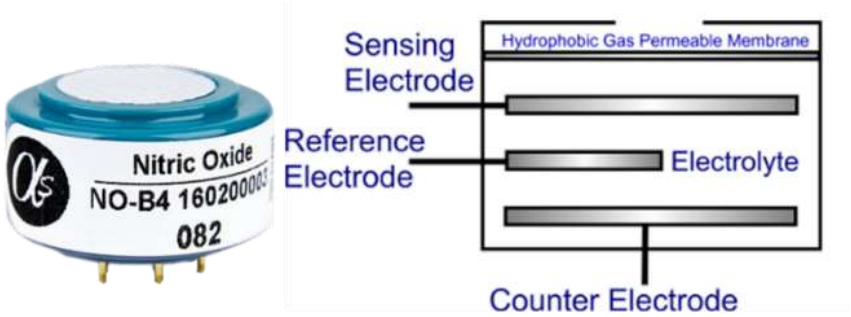

(a)

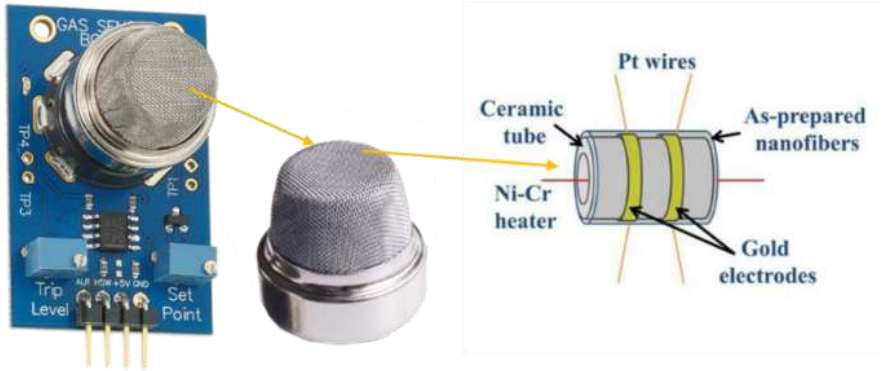

(b)

Figure 2: (a) Electrochemical sensor (b) Chemiresistive sensor

1.6 Materials for Solid State Sensors

There are no limitations to the use of material for solid-state gas sensors. In general, a sensor should have high sensitivity, selectivity and stability. Sensing material choice is greatly influenced by electronic structure, adsorption/desorption characteristics, catalytic activity, band gap, electric conductivity and thermodynamic stability. Graphene fulfils many requirements, primarily sensitivity, selectivity and stability required in sensing materials [11,12]. According to the work of Schedin et al. graphene can provide ultimate sensitivity, because graphene have low electrical noise as compared to conventional semiconductors and fast catalytic electrons transfer [13]. The adsorption of CO on pristine graphene is low, which shows that the pristine graphene cannot provide useful electronic signals for CO sensing. For tailoring the graphene properties for a specific gas like CO, graphene is either doped or combined with two or more materials [14]. In this work we have used both approaches to prepare highly sensitive CO gas sensor. In this research the following composite/materials have been synthesized for CO gas sensing;

- Reduced Graphene Oxide (rGO).
- Nitrogen doped reduced graphene oxide (N-doped rGO).
- Graphene and Metal Oxide (Fe_3O_4 and CoOOH) Composite.
- Graphene and Metal Organic Framework (MOFs) Composites.

1.7 Introduction to Graphene

Graphene have 2D structure which is compose of carbon atoms that are Sp^2 hybridized and arranged in hexagonal pattern. This type of arrangement is called honeycomb structure. Graphene exhibit extraordinary mechanical, electric properties and very high specific surface area. High mechanical strength is due to covalent nature of bonding and small bond length. High electric conductivity and low electrical noise is because of no band gap between valance and conduction band [15]. The electron mobility in graphene is about 100 times greater than any other conductive material, and it has the ability to tolerate high concentrations of electrical current.

Graphene is completely impermeable to all the gasses and have high adsorption capacity. These two properties are highly valuable in gas sensing applications. As graphene is considered “the next wonderful material” however to replace currently used materials in electronics with graphene is still debating. Carbon atoms in graphene

are Sp^2 hybridized, Sp^2 hybridization yield three Sp^2 orbitals that are arrange at 120^o degrees and one un-hybridized orbital which form delocalized electronic cloud just like benzene. [16]

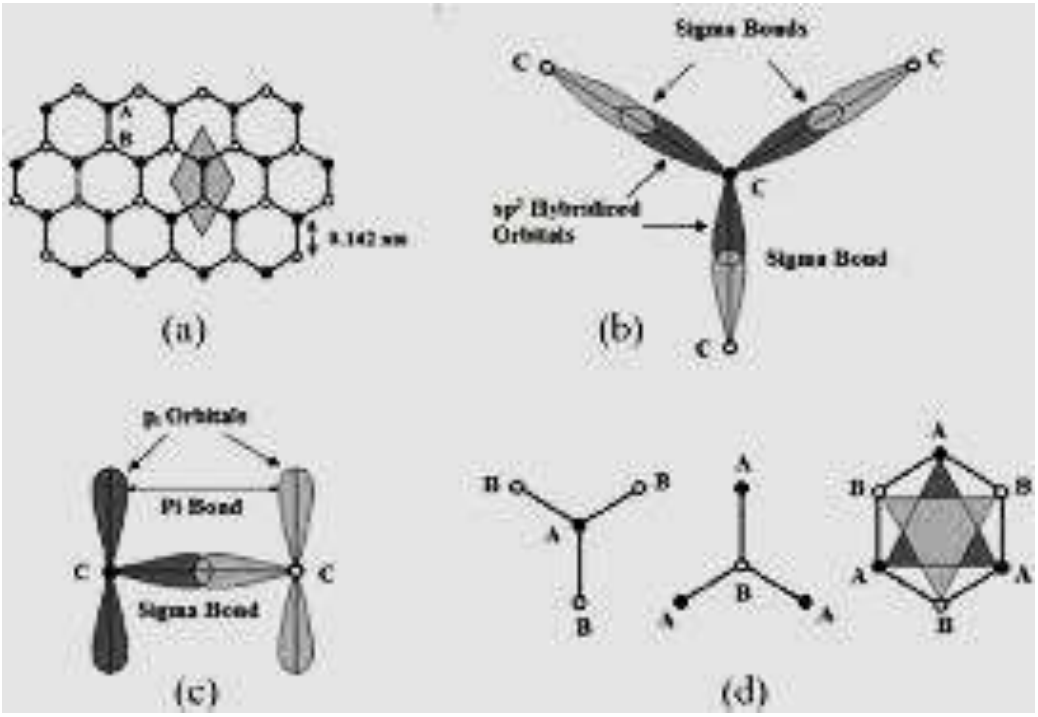

Figure 3: Structure of Graphene

1.8 Routes for Graphene Preparation

In 1859, Benjamin Brodie provided the base for graphene synthesis by chemical method, he studied the reaction of graphite with oxidizing agent such as chlorates [17]. In 1898 L. Staudenmaier rendered the reaction time by using sulfuric acid in reaction mixture of Brodie. In 1958, Hummers and Offeman published graphite oxide preparation using potassium permanganate instead of chlorate which produce toxic ClO [18]. About 90 year after Brodie, Vogt studied the exfoliation of graphene oxide and found cracked sheets using transmission electron microscopy [19]. In 1986, Boehm et al. labeled these bodies as “graphene” [20]. Geim and Novoselov isolated single layer of carbon atoms by mechanical exfoliation using scotch tape and they received Noble Prize for their work [21] and studied the electric properties of graphene. Their work set off researchers to study graphene more for different application.

Graphene can be synthesized by using graphite as raw material or by using any carbon material (methane, ethane, acetylene).

1. The exfoliation method of graphite includes;

- Mechanical cleavage
- Liquid-Phase Exfoliation
- Electrochemical methods.

2. Using Carbon precursor, Chemical Vapor Deposition and Thermal Decomposition of SiC are used.

1.8.1 Chemical Deposition Method

In this process transition metal substrate put in a closed chamber and gradually heated to 1000°C with the continuous flow of feed gas, the carbon atom from hydrocarbon nucleate on the substrate and nuclei grow to give a lager film [22].

1.8.2 Thermal decomposition of silicon carbide

This method utilized the segregation of SiC. This method has the ability to produce large films of graphene. This process involve two steps; annealing of SiC at above 800°C under continuous flow of H_2 or Argon, which cause the sublimation of Si, in second step carbon atoms arrange themselves to give graphene [23].

1.8.3 Mechanical cleavage

Mechanical Exfoliation is called the mother of graphene synthesis because Geim extracted single-layer from graphite using scotch-tape. He stick graphite on a piece of tape and cleaved it with other sticky tape until invisible powder left on the starting tape and then transferred it to silicon dioxide substrate.[21]

1.8.4 Electrochemical method

In this method boro-silicate glass pressed on graphite layer at 200°C, and the voltage of 1700-1800V is applied. The electric field pull the layers of graphite apart and deposited on glass plate. [24]

1.8.5 Exfoliation of Graphite

Exfoliation of graphite is most convenient method to produce graphene. There are two ways of graphene synthesis by this method;

a) Exfoliation of Graphite by using Solvent.
b) Exfoliation of Graphite by Oxidation.

a. Exfoliation of Graphite by using Solvent

Process involves three step; in first step the graphite is mixed in a solvent that increase the distance between the graphite layers, in second step mixture is ultra- sonication to

split graphite layer into individual platelets. Final step is the purification of the product by removing solvent [25].

b. Exfoliation of Graphite by Oxidation

Oxidation route of graphene synthesis by using graphite as starting material is largely used method. Oxidation of graphite is done by using strong oxidizing agent like $KMnO_4$ and concentrated sulfuric acid followed by reduction using strong reducing agent like ascorbic acid or the salts of hydrazine to give graphene usually called reduced graphene oxide (rGO). [18]

1.9 Reduction of GO

During oxidation of graphite different functional groups attached to GO sheets. These functional groups have different binding energies depending upon the type and location. To obtained graphene, these functional group should be removed, the graphene obtained by the removal of functional groups from GO is called reduce graphene oxide (rGO).

Many methods are available to remove these groups, some important and vastly used are given in table 1.3. [26-46]. Thorough reduction of GO is very tough to attain, but for large scale synthesis and applications graphene production through GO is very attractive. The structure of rGO sheets is given in figure 4.

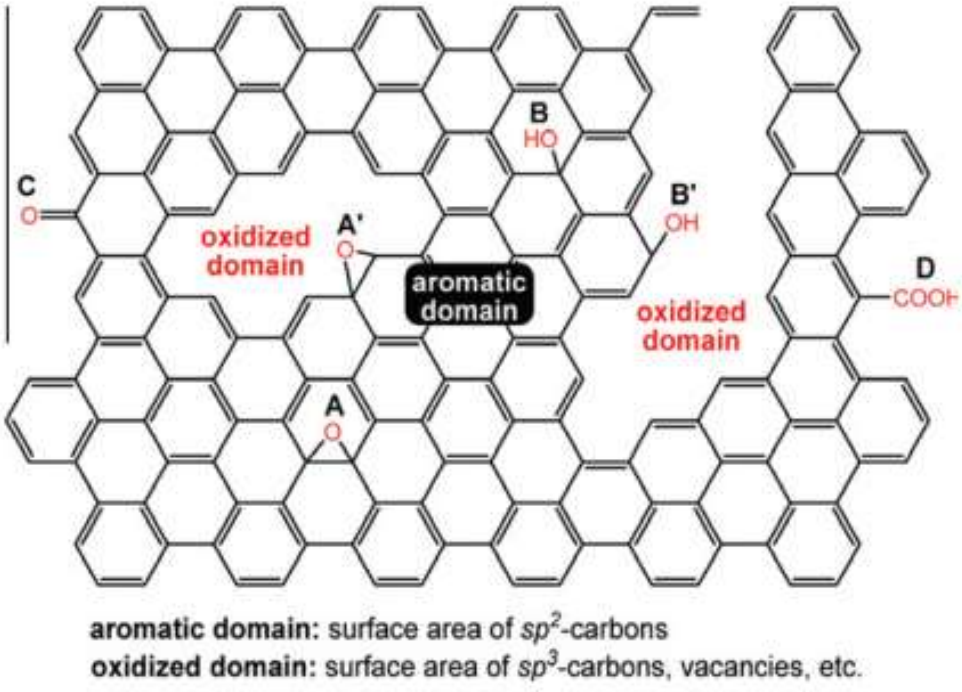

Figure 4: Structure of rGO sheet

Table 1.2 [26-46] A comparison of GO reduction methods			
Advantage	**Disadvantage**	**Electric conductivity**	**Carbon/Oxygen Ratio**
Thermal Reduction			
Different level of reduction can be achieve by varying temperature.	Small size, wrinkled graphene sheets. 30% yield. Large energy consumption	Depend upon reduction temperature, typical mean value is10–23S/cm. 500^{o}C 50 S/cm, 700^{o}C 100 S/cm 1100^{o}C 550 S/cm.	Depend upon the temperature. At 500 ^{o}C ratio is 7. At 750^{o}C ratio is 13.
Radiation Reduction			
Uniform and rapid reduction.	Expansive and not suitable for bulk production	Photo-irradiation =10 S/cm Laser = 256 S/cm	----
Photocatalytic Reduction			
Green and Sustainable, Low waste production.	High level of reduction cannot be not be achieved. Use UV- light source.	Electric resistance around 150 (kΩ/sq)	----
Electrochemical Reduction			
No special chemical agent Room temperature No toxic waste	Large scale synthesis is costly and difficult.	85 S/ cm	23.9
Chemical reagent reduction			
Mass production, cheaper and easily available	Chemical waste is produced	Hydrazine 99.6 S/ cm $NaBH_4$ 16.6 S/cm. Ascorbic acid 77 S/cm Hydroiodic acid 300 S/cm	Ration ranges from 13-15 depending upon reducing gent used
Solvothermal Reduction			
Green, less toxic and produce a stable and well dispersion rGO sheets	Time consuming, high pressure and less reduction than other methods.	Electric resistance depend on solvent used DMF 10^{5} –10^{6} Ω/sq NMP 3.74 S/cm	14.3

1.10 Graphene Doping

Heteroatoms doping is the best method to regulate semiconducting properties of graphene. Because of similar properties, Nitrogen atom is natural heteroatoms for doping. [47-51].

Different nitrogen doping methods could produce different properties. Many synthesis methods are available as given below [52-60];

- Chemical Vapor Deposition (CVD)
- Thermal Annealing
- Pyrolysis
- Solvothermal Method
- Arc-Discharge
- Plasma Treatment
- N_2H_4 Treatment
- Hydrothermal Method
- Wet Chemical Synthesis

Graphene doping with nitrogen produced different kinds of groups in lattice as shown in figure 5, Pyridinic, Quaternary and Pyrrolic. [61-63].

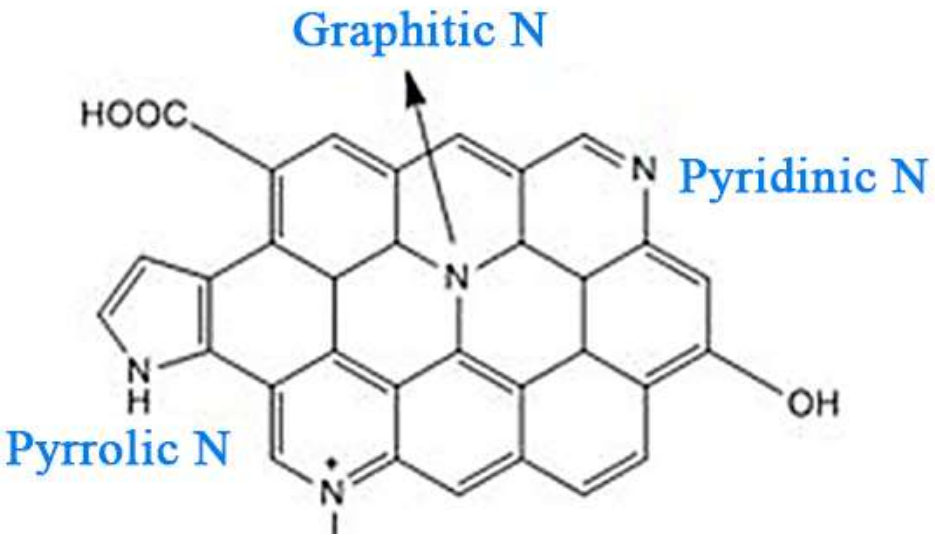

Figure 5: Structure of Nitrogen doped rGO sheet

1.11 Metal Oxide Nanoparticles

Metal oxides nanoparticles based gas sensors have been largely investigated till now. It has been well known that metal oxides alter their electrical resistance with the change in gas composition in surroundings [64]. In 1968, Taguchi commercially

produced gas sensor for the sensing of explosive gases. The sensor was made of SnO_2 thick film, the detail structure of that sensor is given in figure 6. Other than SnO_2, TiO_2, In_2O_3, WO_3, ZnO, Fe_2O_3 have been studied for chemical sensing.

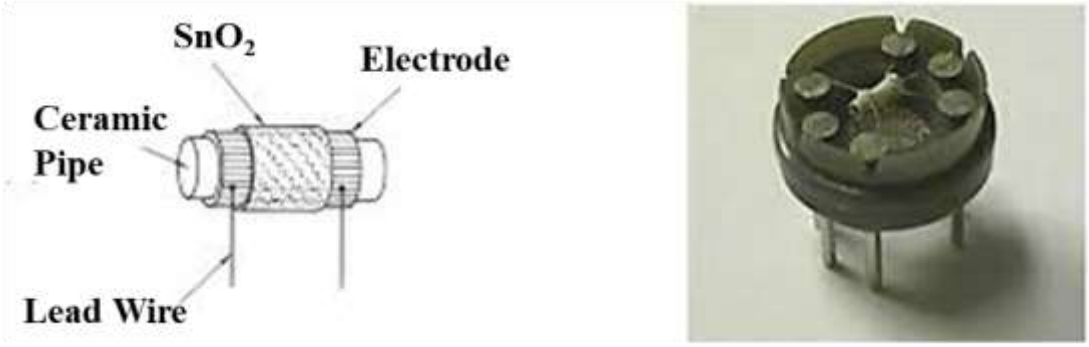

Figure 6: Schematic picture of Taguchi chemoresistive gas sensor

Moreover, noble metals composites with metal oxides have been studied to enhance sensitivity and stability. In 1991 Yamazoe [65] published most important findings. He proved that with the reduction in crystallite size, sensor performance is largely increase. Metal oxide gas sensor took new turn with discovery of metal oxide nanowires. This shifted the research community to synthesis different shaped metal oxide nanoparticle for gas sensor.[66] With the increase in interest of researchers in graphene, rGO/ Metal Oxide Nanocomposite have shown great potential for next generation metal oxide gas sensors with high stability, long lifetime and low-operating temperature [67].

1.12 Metal Organic Frameworks (MOFs)

MOFs are porous coordination polymer with exceptional properties like permanent nanoscale porosity with extraordinary surface area, uniform and tunable pore size, and ability of being functionalized. These properties make them better than conventional porous materials. MOFs are under intensive studies and extensively use in gas storage, separation, catalysis and chemical sensors. Typically, MOFs are synthesized by compilation of metals and multi dentate organic linkers by coordination bonds. Most MOFs have 3 dimensional structure incorporating various pores and a number of open channels. [68-70].

MOFs are formed by unique coordination reaction of metal ions and organic linkers. MOFs network geometry relies heavily on the organic ligands properties and metal synchronization. Particularly, new MOFs can be set up by changing the linker bridge

or its functionalization, without changing the original topology of the MOF. Coordination spots are offered by the transition metal ions to the organic ligands [71]. Ligands are generally multidentate bridging linkers, containing an extensive choice of linking sites, they have, exceptional to its topology, direction of organic linkers and binding strength. Rigid ligands will be responsible for the physical topologies during synthesis.

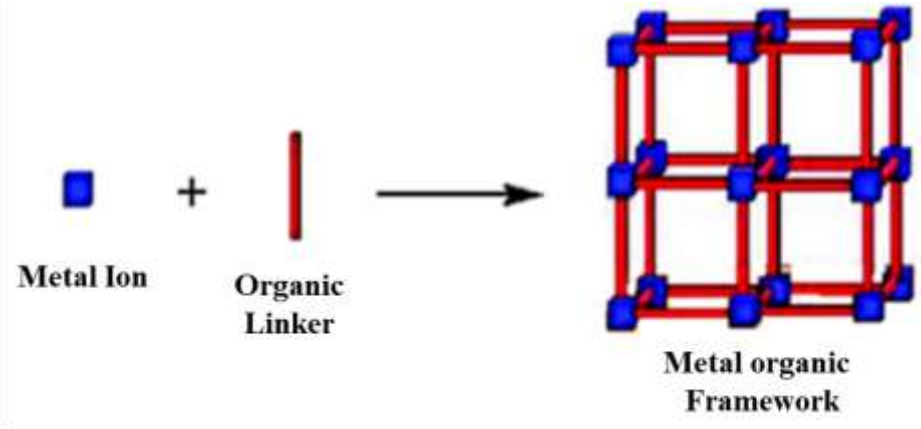

Figure 7: MOFs synthesis reaction

MOFs can be synthesized by utilizing numerous methods including hydrothermal, room temperature crysallization, solvothermal, microwave heating, vapor diffusion, direct mixing and so on. The solvothermal and room temperature synthesis methods for MOFs production are usually utilized. These synthesis routes also tend to lead to different properties of MOFs. For example, MOFs synthesized by solvothermal method have larger particle size than room temperature synthesis method. [72].

1.13 Sensing Mechanism

A general sensing mechanism involves the combination of physisorbed gas with oxygen, which is chemisorbed on the sensing material surface.

As oxygen chemisorbed on the surface it forms many ions as shown below.

$$O_2\,(gas) \leftrightarrow O_2\,(ad) \leftrightarrow O_2^-\,(ad) \leftrightarrow O^-\,(ad) \leftrightarrow O^{2-}\,(ad) \leftrightarrow O^{2-}\,(lattice)$$

Reducing gas CO interacts with O^- as show equation below;

$$O^- + e^- \rightarrow O^{\infty}\ (chemisorbed)$$

When sensor is exposed to CO gas,

$$CO\,(g) \rightarrow CO\,(physisorbed)$$

it react on the surface as follow and release electron (generate electric signal);

$$CO\ (physisorbed) + O^{-} \rightarrow CO_2 + e^{-}$$

$$CO\ (physisorbed) + O^{=} \rightarrow CO_2 + 2e^{-}$$

CO release electrons on interactions and cause decrease in resistance of overall material. The nitrogen doped graphene or graphene in composite provide energetically favorable sites and increase the sensitivity.[73]

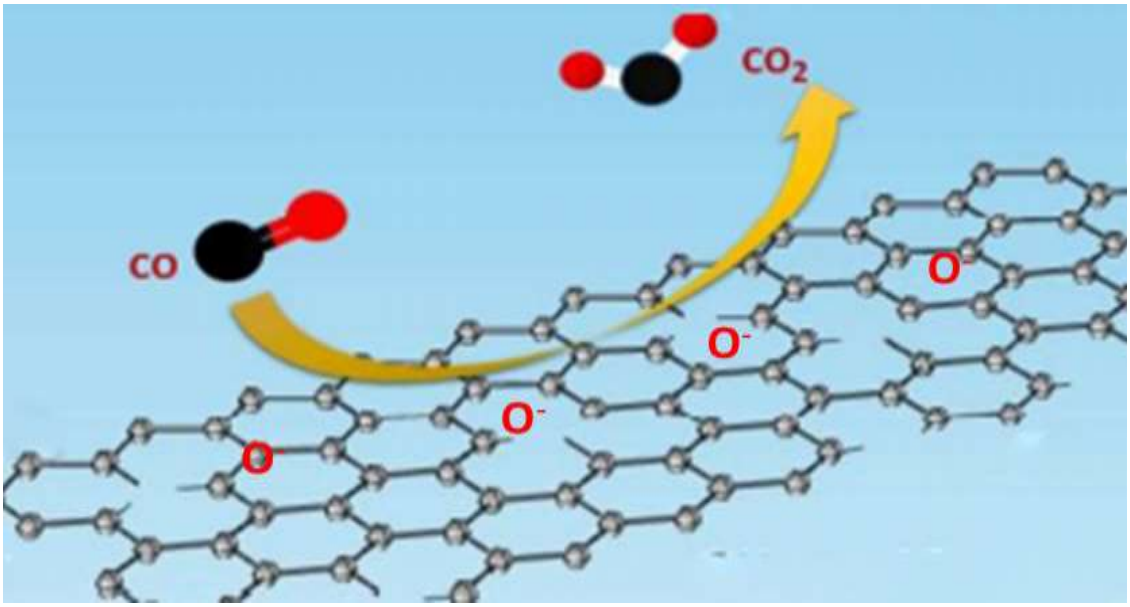

Figure 8: Gas sensing Mechanism

CHAPTER 2

Literature Review

2.1 Carbon monoxide Gas Sensors

In 1990s CO was detected using a white mat of $K_2Pd(SO_3)_2$ which change its color in the presence of CO. This type of detector give only visual warning and did not provide a quantitative measurement of CO level. Although this type of sensor has low cost but provide low protection. With the increase in death rate due to CO poisoning, audible sensors become important. Solid state gas sensors (described in section 1.) which provide an audible alert of CO presence developed to save human lives.

Electrochemical sensors are highly accurate, operate at room temperature but have a complex structure, high cost and low lifetime. Because of simplicity, low cost and a large range of application CO chemi-resistive sensor is under a lot of interest. Efforts are on to develop sensing material that improves the sensitivity of chemi-resisitive sensor and operate at room temperature [9].

There are no limitations to the use of material for solid-state gas sensors. In general, a sensor should have high sensitivity, selectivity and stability. Graphene is considered "the next wonderful material" the electron mobility in graphene is about 100 times greater than any other conductive material, and it has the ability to tolerate high concentrations of electrical current. Graphene is completely impermeable to all the gasses and have high adsorption capacity. These two properties are highly valuable in gas sensing applications [11-13].

2.2 Graphene for Carbon Monoxide Gas Sensor

Graphene has been studied for many gases as shown in table 2.1, but for CO, graphene has not got much attention. It can be seen from table 2.1, for the detection of different gases graphene is either doped or combined with other materials for selective detection of particular gas. Adsorption of CO on the pristine graphene cannot provide useful electronic signals to fabricate a CO sensor, to make graphene responsive for CO, graphene is doped with nitrogen and its composites with metal oxide nanoparticle and metal organic framework are prepared for CO sensor fabrication. Also Graphene synthesized by graphite oxidation generates natural defects that also increase the sensing characteristic of graphene.

Table 2.1: Literature Review of Graphene used in Gas Sensing Application			
Authors	**Year/Journal**	**Gas Detection**	**Type of Graphene**
F. Yavari et al.[74]	2012 Applied Physics Letters	Ammonia (NH_3) gas	Graphene films synthesized by CVD
L. Huang et al.[75]	2014 ACS Applied Materials & Interfaces	Nitrogen Dioxide	Sulfur functionalized rGO and composite with Ag nanoparticles
K.R.Nemade et al. [76]	2013 Journal of Modern Physics	Carbon Dioxide Detection	Graphene/Y_2O_3 quantum dots (QDs)
K.R.Nemade et al. [77]	2014 Optical Materials	Carbon Dioxide	Graphene/Sb_2O_3 QDs Graphene/Al_2O_3 QDs
J.L.Johnson et al. [78]	2010 Advanced Materials	Hydrogen Detection	Pd-coated and multilayered Graphene.
Z. Wu et al. [79]	2013 IEEE Sensors	Methane Detection	Graphene nanosheets/PANI nanocomposite
L. Tang et al.[80]	2010 Chemical Communications	2,4,6-Trinitrotoluene (TNT) Detection	Graphene synthesized by electrophoretic techniques
L. Zhou et al.[81]	2013 Nanoscale	Hydrogen Sulfide	Ag-decorated Graphene composite

Among many doping atoms nitrogen (N) atoms significantly change the performance of graphene. For example, increase in charge distribution of graphene and “active

region" on the surface of graphene. These activated region contribute in catalytic activity like oxidation and reduction reactions in sensors, supercapacitors and batteries. Nitrogen doping cause the replacement of carbon atom by nitrogen in the graphene lattice, which gives graphene novel semiconducting properties for example change in band gap and increase in electrons or holes concentration. Recently, Nitrogen-doped graphene is largely investigated in fuel cells, batteries, supercapacitors and medical field. By now nitrogen doped graphene is growing rapidly. Peng et al. synthesized nitrogen doped graphene for electro-catalyst in fuel cell [82].

MA CongCong [83] showed through mathematic modeling that Nitrogen doping in graphene favors the selective adsorption of CO and CO molecule physisorbed on N-C bonds with high electrons transfer than other gases, which make N-doped graphene highly selectively for CO sensing. In this research nitrogen doping is carried out by using ammonium nitrate as nitrogen source and fabricated senor showed very high sensitivity towards CO.

2.3 Graphene and Metal oxide Composites for CO Sensing

The current semiconductor gas sensor required high temperature for the operation. The operation at elevated temperature cause the fusion of grain boundaries of nano-metal oxides particles which effect the stability and life time of sensor. Moreover these sensors required heating arrangements and power consumption for heating. Although these sensors have high sensitivity but their use for certain conditions are restricted because of their low conductivity, low stability and sophisticated design [84-86].

Metal oxide gained considerable attention for the development of CO chemiresistive sensor. Among the many nanomaterials metal oxide like In_2O_3, Co_3O_4, Fe_3O_4, SnO_2 and CoOOH have been largely investigated for CO gas sensor as described in Table 2.2 but there are many problems associated with metal oxide sensors like poor sensitivity, selectivity and high operating temperature which lead to high power consumption, restriction of use in remote areas and risk of explosion in the presence of explosive or flammable gases.[87-90]

Use of precious metals has been investigated for CO sensor for example, Fu et al. [90] decreased the In_2O_3 operating temperature and enhanced the sensing properties like sensitivity, response time and selectivity by incorporation of In_2O_3 nanoparticles into

Au matrices and Beomseok Kim prepared Pd centered sensor for CO detection at room temperature [87].

Table 2.2: Literature Review of Materials used for CO sensing

Authors	**Year/Journal**	**Key Findings**	
		Material	**Temperature, Response Time, Sensitivity, Problem**
J. F. Chang et al. [91]	2002 Sensors and Actuators B: Chemical	ZnO with Al doping	400°C, 5s, 61.6%, High Operating Temperature
J. H. Yu et al. [92]	2001 Sensors and Actuators B: Chemical	CuO- and ZnO-doped SnO_2	160°C, 23%, High Operating Temperature
Ren-Jang et al. [93]	2006 Sensors and Actuators B: Chemical	CoOOH	80°C, 1min, High Operating Temperature
H. Y. Lai et al. [94]	2012 Journal of Materials Chemistry	Pt−In_2O_3 Pd−In_2O_3	RT, 5s , 60%, Expensive Metal
N. Du et al. [95]	2008 Chemical Communications	CNT/Au/ SnO_2 nanotubes	RT, 20s, 70%, Expensive Metal
Arunkumar et al.[96]	2017 Sensors and Actuators B: Chemical	ZnO/Au nanostars	RT, 40s, 55%, Expensive Metal
H. Kim, et al. [97]	2016 Chemical Communications	RGO/Au/ SnO_2	RT, 18s , 87%, Expensive Metal

2.4 Graphene and MOFs Composites for CO Sensing

Researchers suggested that not only the particle size of sensor's material but also the porosity of material effects the sensitivity of gas sensors. The sensitivity increase with decrease in particle size and increase in porosity of materials [102].

Recently, Lee suggested that the combination of metal with porous structure, increase the available active sites for gas chemisorption and improve the sensing properties at room temperature [103]. Metal Organic Frameworks (MOFs) consist of organic linker and active metal sites are considered to be promising candidates for gas sensor. The porosity of MOFs enable the reversible adsorption of incoming species and open metal sites contribute to increase the sensitivity of the sensor. However inherent poor conductivity make it difficult to use MOFs alone in gas sensor. Therefore to overcome the electron transport rate, graphene is incorporated into MOF to use them effectively in gas sensors.[104-105].

Among many MOFs, ZIF-67 is thermally and chemically stable and can be produced at low temperature using environmental friendly method. Coupled with relative ease of synthesis, ZIF-67 contain cobalt in +3 oxidation state, which is an active metal for CO oxidation. [106] Currently, Wenlan [107] showed that ZIF-67 is selective for CO adoption and catalytic oxidation.

ZIF-67 are consist of cobalt metal and Imidazolate linkers. With the loss of a proton IM is formed and make bonding at 145° angle with metal and form M-IM-M. This type of bonding is similar to the bonding of Silicon-Oxygen- Silicon (Si-O-Si) in the zeolites as described in figure 9 [108].

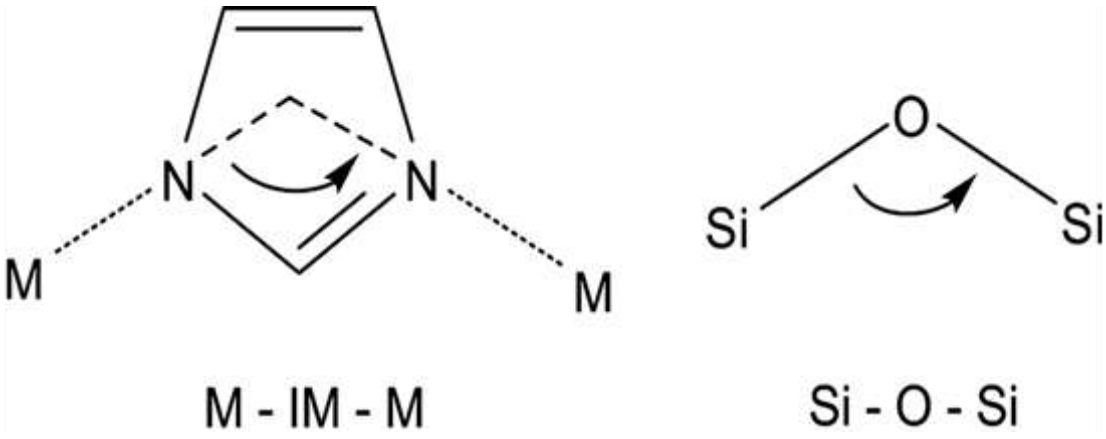

Figure 9: Bonding in ZIF-67

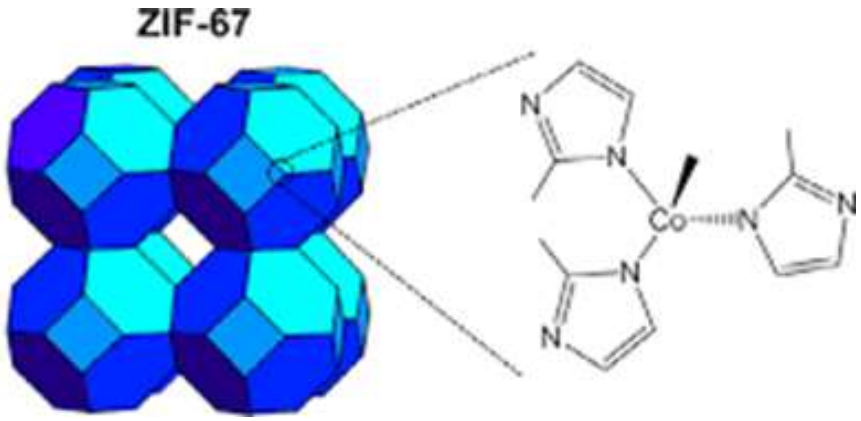

Figure 10: Linking of ligand in ZIF-67 crystal

Another MOF with Nickel as activate metal for CO oxidation and 1,4-benzenedicarboxylic acid (BDC) linker is also studied in this research. In this Nickel-based metal–organic framework (Ni-BDC), nickel cation have high oxidation state and high oxidation is attributed to higher catalytic CO oxidation [109]. Figure 11 explains the structure of Ni-BDC.

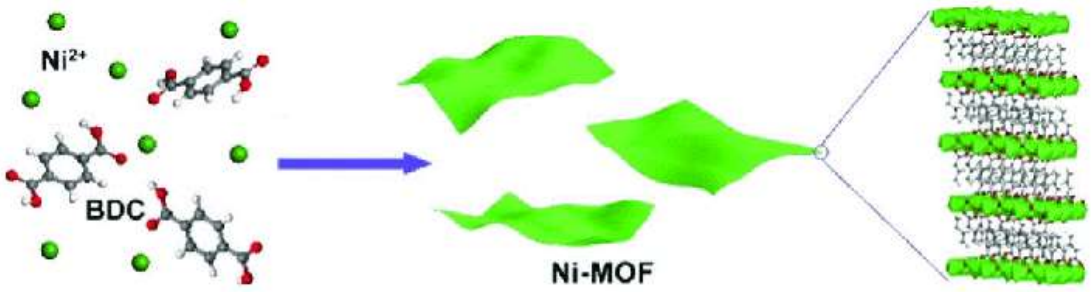

Figure 11: Ni-BDC-MOF Structure

Chapter 3

Experimental

3.1 Synthesis of GO

Hummers [110] described a noval process of graphite oxidation in 1958, most frequently used these days, by improving the work of Brodie and Staudenmaier. In Hummer's method, $KMnO_4$ and $NaNO_3$ in the presence of H_2SO_4, oxidized graphite to graphene oxide. But, this routine have some drawbacks, release of NO_x and presence of Na^+ and NO^{3-} ions.

In 2010 James M. Tour [111] improved the Hummer's method by increasing the amount of H_2SO_4 and removed the $NaNO_3$ from oxidation reaction and make the reaction non explosive but increasing the reaction time and high consumption of the oxidants.

Several modification have been done to increase the yield of Hummer's method to increase yield. A novel modified hummer's method is used in this research for GO synthesis.

Material: Graphite powder, Sulphuric acid (97%), Phosphoric acid H_3PO_4 (87%), Potassium Permanganate ($KMnO_4$), $NaNO_3$, Hydrochloric acid (HCl 35%), H_2O_2 (30%) acquired from Sigma Aldrich & Ethanol (≥99.5%.) from MERCK. All reactants and solvents have been used without further purification.

Procedure: In first step the concentrated H_2SO_4 and H_3PO_4 (108:12ml) are mixed in a flask than 5g powder graphite added in the acid mixture under continuous stirring. The addition of phosphoric acid (H_3PO_4) along with H_2SO_4 helps to form more intact graphitic basal planes during oxidation. When homogenous black colored solution formed, 2.5g of $NaNO_3$ was added and temperature of reaction decreased to 0 °C by using ice bath. The addition of $NaNO_3$ in reaction increase the interlayer distances to a smaller extent before oxidation and helps the oxidation on the basal planes. 15g $KMnO_4$ was added in small lots and mixture was stirred for 1hr.

In last step of heat treatment, temperature was increased to 40°C and stirred for another 60 min. After heat treatment 400 mL distill water was added slowly and the resulting mixture was left to cool. After cooling, 3 mL of H_2O_2 was added in the reaction

mixture and stirred for 30min to remove unreacted $KMnO_4$ and color of reaction mixture turn to brown.

The brown solid material was washed with 200 mL of 30% HCl than with distill water by centrifugation until pH of supernatant reached to 6 and finally with 200 mL of ethanol. The product was vacuum-dried overnight at 60˚C. The sequence of all the steps involved in the synthesis of GO is describe in figure 12.

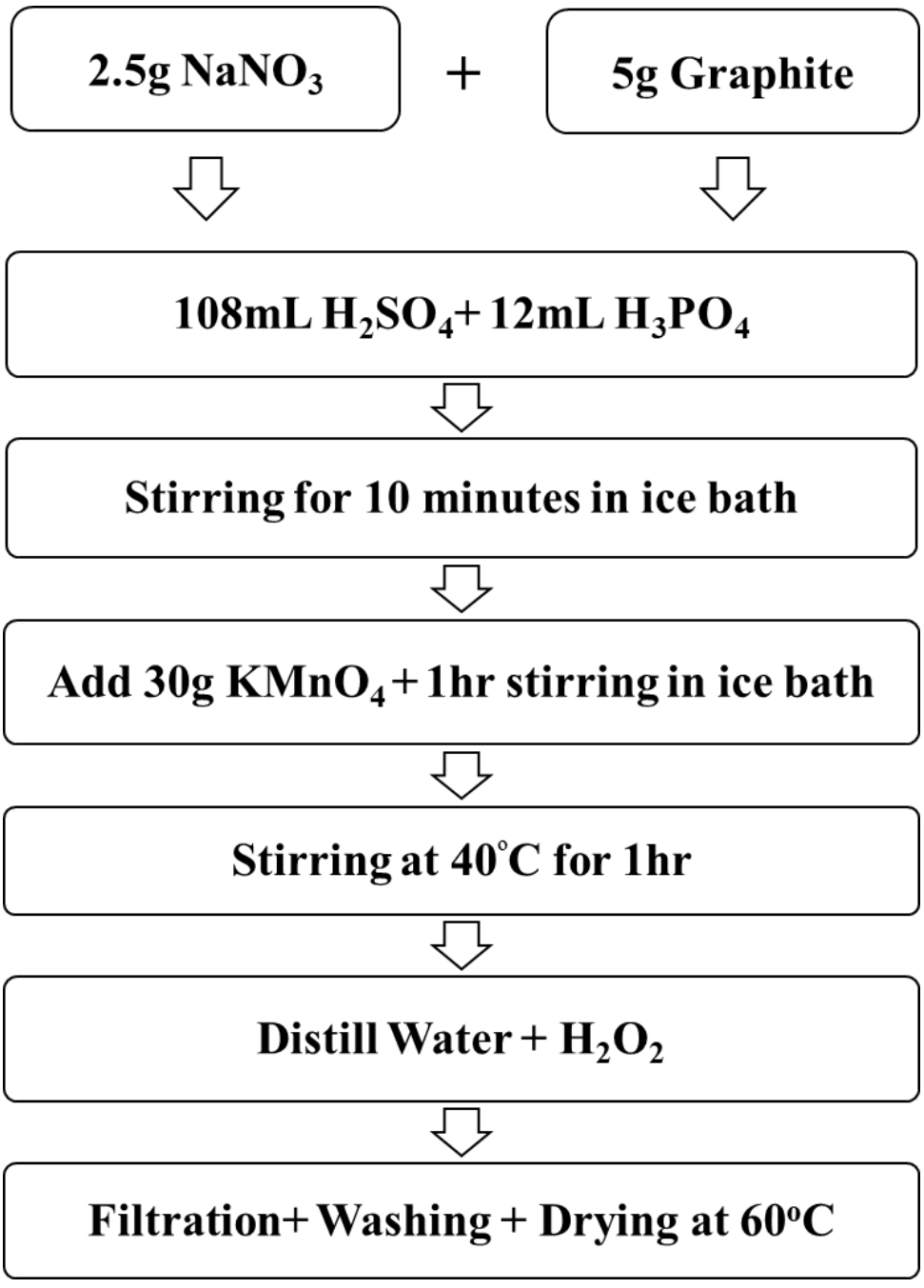

Figure 12: Scheme of GO Synthesis

3.2 Synthesis of rGO

Material: GO powder (prepared by above Method), L-Ascorbic Acid, N,N-dimethylformamide (DMF) and Ammonia Solution (25%) bought from Sigma-Aldrich with best quality assurance and were used without further processing.

Procedure: The reduction of GO was performed using ascorbic acid a greener reducing agent according to the method described by Jiali Zhang [112]. 3g of graphene oxide was taken in a flask and sonicated in 50ml of water for 1hr. 100ml of DMF/NMP added in solution and sonicated until GO sheets are complete dispersed. 1ml of 25% ammonia solution added into GO dispersion under vigorous stirring. Afterwards 1gram of ascorbic acid added for reduction and reaction mixture stirred for 24hr.

After 24hr stirring the color of the mixture will turn to black. The resulting rGO was purified and dried. The sequence of synthesis is also explained in figure 13.

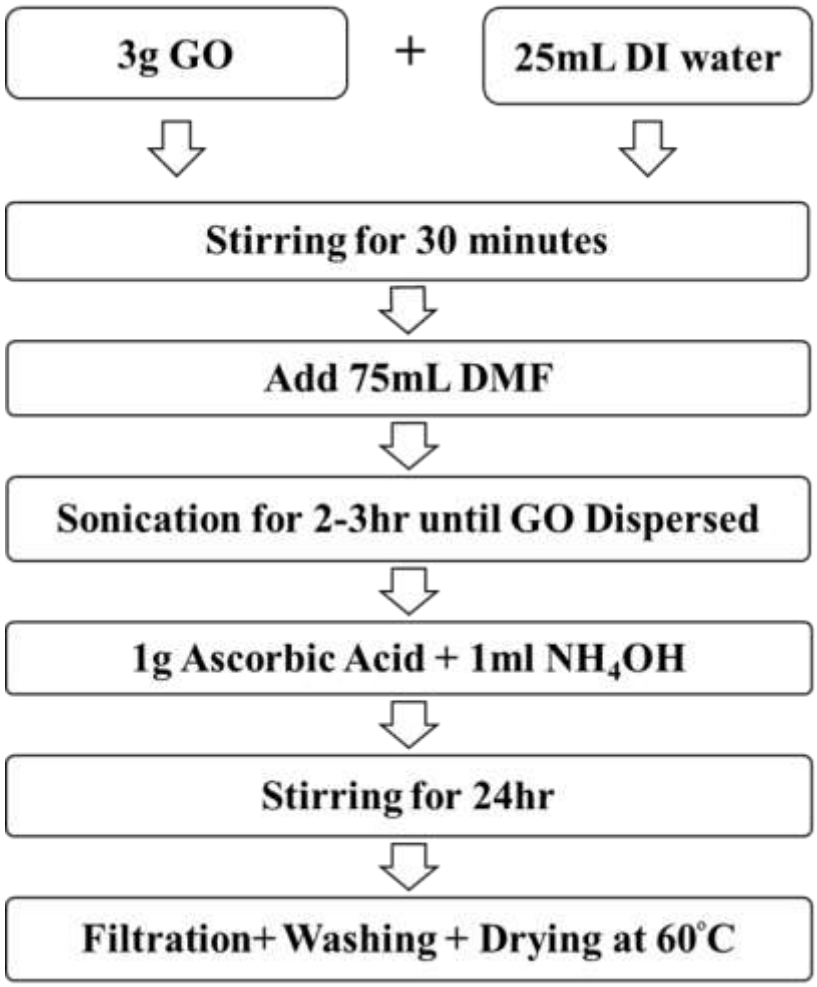

Figure 13: Scheme of rGO Synthesis

3.3 Synthesis of N-doped rGO

Material: GO powder, ethanol (99.5 %.) was purchased from MERCK. Ammonium Nitrate (98%) Sigma-Aldrich.

Procedure: Nitrogen doping was carried out by using method described by Hongqi [113].1 gram of GO was added in 25 mL of ethanol and sonicated until completely dispersed. 1.0 g of ammonium nitrate was added in sonicated GO solution. After evaporating ethanol, mixture was calcined at 350^{o}C for 1 hr. Resulting product washed with ethanol and DI water and dried in an over at 80^{o}C overnight.

The sequences of all the steps involved in the synthesis of Nitrogen Doped rGO is given in figure 14.

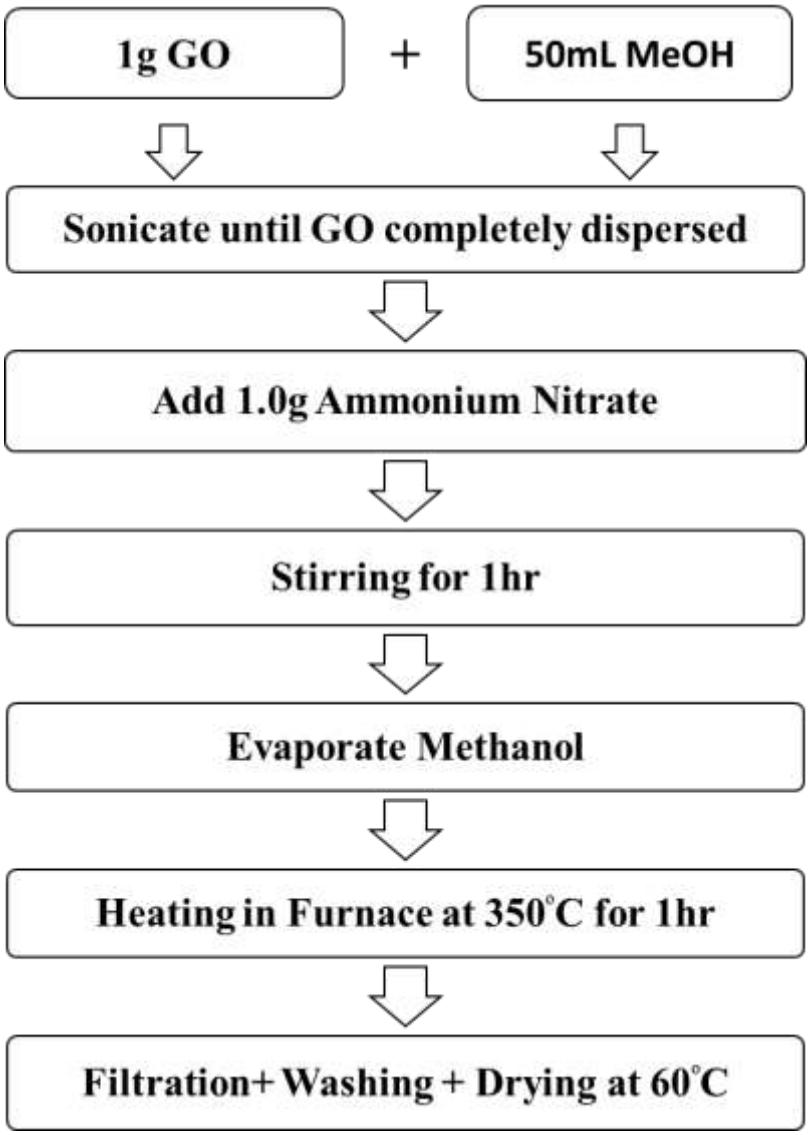

Figure 14: Scheme of N-doped rGO Synthesis

3.4 Synthesis of CoOOH Nanoparticle and rGO/CoOOH Composite

Material: NaOH (97.0%) and Cobalt nitrate hexahydrate (99.999%) were bought from Sigma Aldrich and deionized (DI) water produced in lab.

a) Synthesis of Cobalt Oxyhydroxide (CoOOH) Nanoparticle:

The synthesis of CoOOH done by method describe by Ren-Jang [93] and shown in Figure 15. 0.1g NaOH added in 25ml of water under continuous stirring (Solution A). Next 0.5g $Co(NO_3)_2 \cdot 6H_2O$ added in 50ml water separately (Solution B). In next step Solution A was dropwise added into Solution B until pH reached 9 and pink color $Co(OH)_2$ precipitate are formed. In last step $Co(OH)_2$ precipitates heated in an oven to get CoOOH. The sequences involved in the synthesis of CoOOH is explained in figure 15.

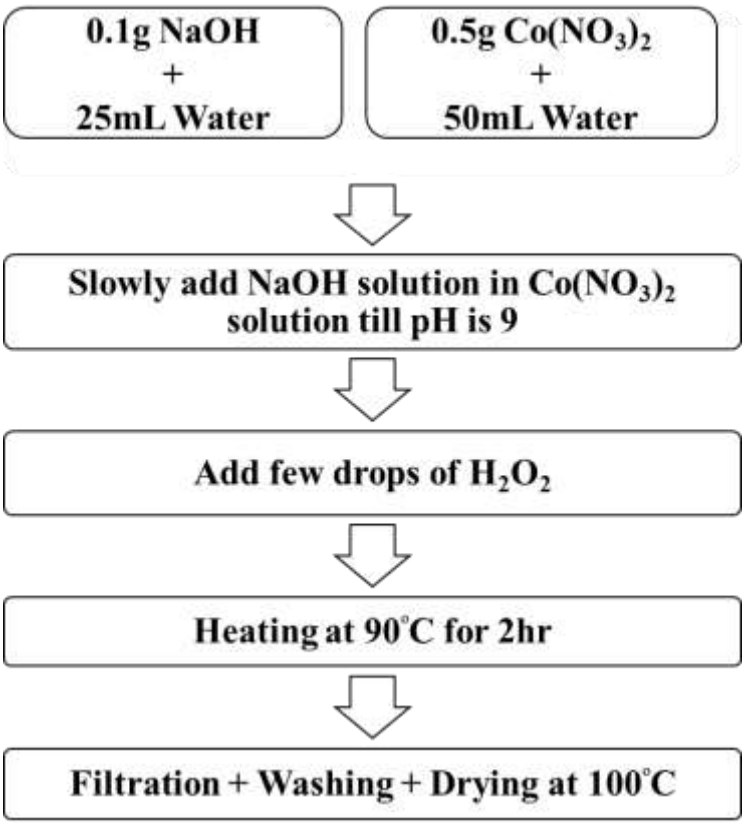

Figure 15: Scheme of CoOOH Synthesis

b) Synthesis of rGO/CoOOH Composite:

For the synthesis of rGO/CoOOH, 3g of GO was dispersed in 50 ml of ethanol. 1 g of CoOOH nanoparticles were added in GO solution and sonicated for 3h. After evaporating ethanol, sonicated mixture heated to 250 ^oC for 1 hour. Subsequently, the resulting composite purified and dried.

3.5 Synthesis of Fe_3O_4 and rGO/ Fe_3O_4 Composite

Material: Graphene Oxide powder (prepared by above Method), Ferric Chloride Hexahydrate ($FeCl_3 \cdot 6H_2O$) of Merck, Sodium Acetate (NaAc), Sodium Dodecyl Benzene sulfonate (SDBS) & Polyethylene Glycol (PEG) of Sigma Aldrich . DI water

a) Synthesis of Fe_3O_4 Nanoparticles

Method described by Tifeng Jiao [114] is used for the synthesis of iron oxide nanoparticles. 1.35 g Ferric chloride hexahydrate was dissolved in ethylene glycol (25 mL), followed by the addition of 0.8g NaOH under continuous stirring. After 30 mins 1.0g polyethylene glycol added into the mixtures and left for stirring for 60 min.

Next solution was autoclaved at 220 °C for 24 h. After the reaction was completed, Fe_3O_4 nanoparticles was purified and then drying. The sequences of all the steps involved in the synthesis of Fe_3O_4 nanoparticles is given in figure 16.

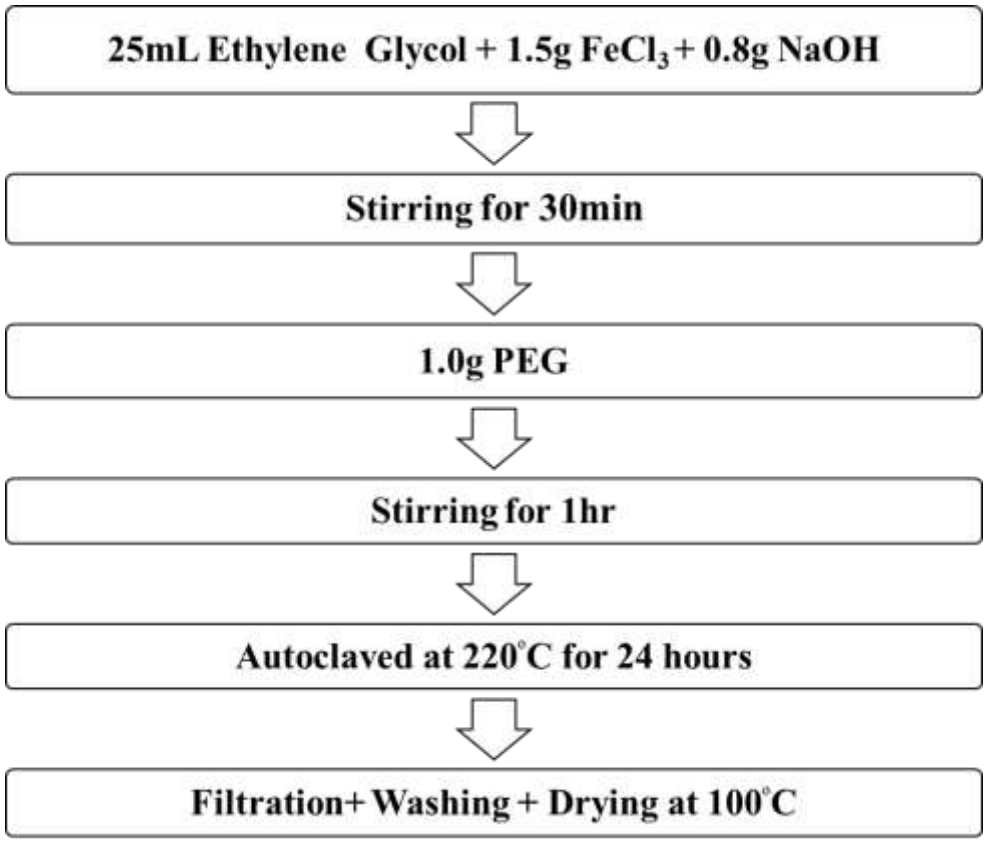

Figure 16: Scheme of Fe_3O_4 Nanoparticles Synthesis

b) Preparation of rGO/ Fe_3O_4 Nanoparticle Composite

For the preparation of composite, 1g of as prepared GO was sonicated in 100 mL water. Next 0.5g of Fe_3O_4 was added in above GO solution and sonicated of 3h. After

sonication, the homogenous solution was autoclaved at 120°C for 12h. Obtain product was purified and dried. The sequence of all the steps involved in the synthesis is also explained in figure17.

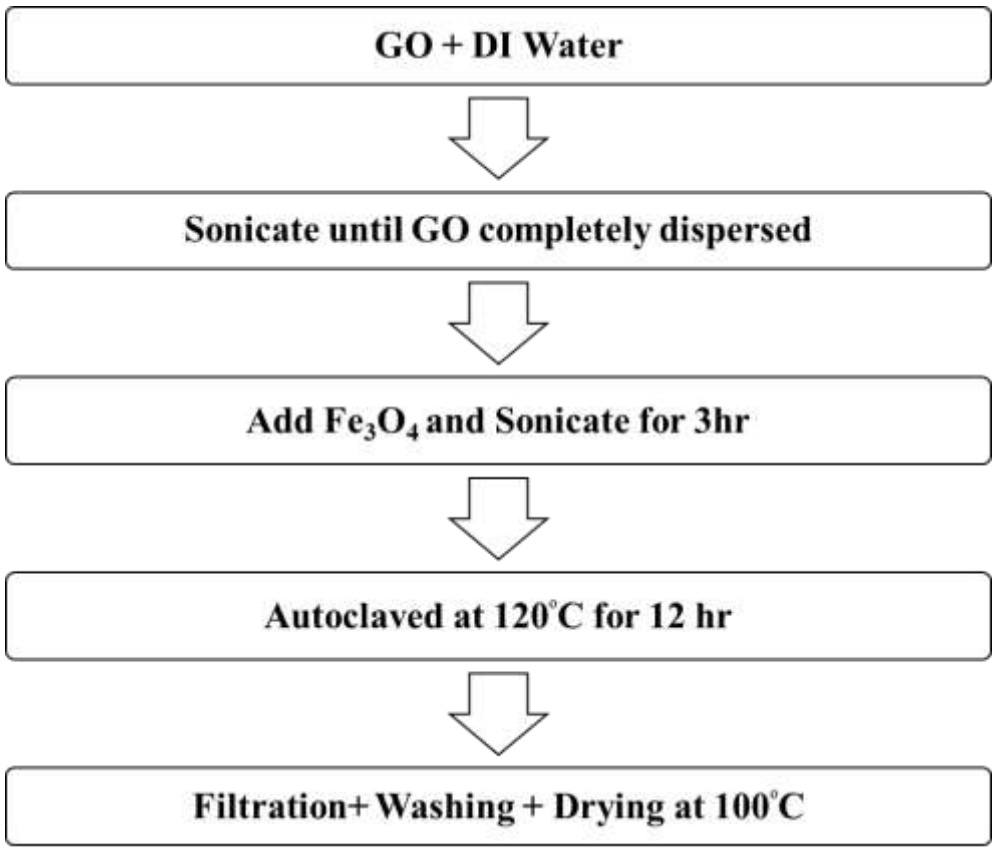

Figure 17: Scheme of rGO/Fe_3O_4 hybrid Synthesis

3.6 Synthesis of ZIF-67 and rGO/ZIF-67 Composite

Material: rGO powder (prepared by above method), Cobalt nitrate hexahydrate was of 97% purity and manufactured by DAEJUNG. The 2-Methylimidazole (MIM) of 99% purity was purchased from MERCK. Methanol and Ethanol were also purchased from MERCK. Both having purity ≥99.5%. All these chemicals were used as per received.

a) Synthesis of ZIF-67

ZIF-67 synthesized by a room temperature crystallization method as described by Wenlan Ji [107]. 484.3mg $Co(NO_3)_2 \cdot 6H_2O$ mixed in 50 mL methanol (Solution A). 500.13 mg MIM mixed in 50 mL methanol (Solution B). Solution A and B mixed together and reaction take place at room temperature for 24hr. Obtained ZIF-67 purified and dried. The sequence of all the steps involved in the synthesis of ZIF-67 is also explained in figure 18.

b) Synthesis of rGO/ ZIF-67 composite

The rGOZIF-67 composite formulated by method as described by Wenlan Ji [115]. rGO was added in 50 mL of ethanol and sonication until rGO completely dispersed. Synthesized ZIF-67 was added in above rGO solution directly and sonicated for 80 min. Subsequently, sonicated solution filtered to remove methanol and dried at 60ºC. The sequence of all the steps involved in the synthesis of rGO/ ZIF-67 is given in figure 18.

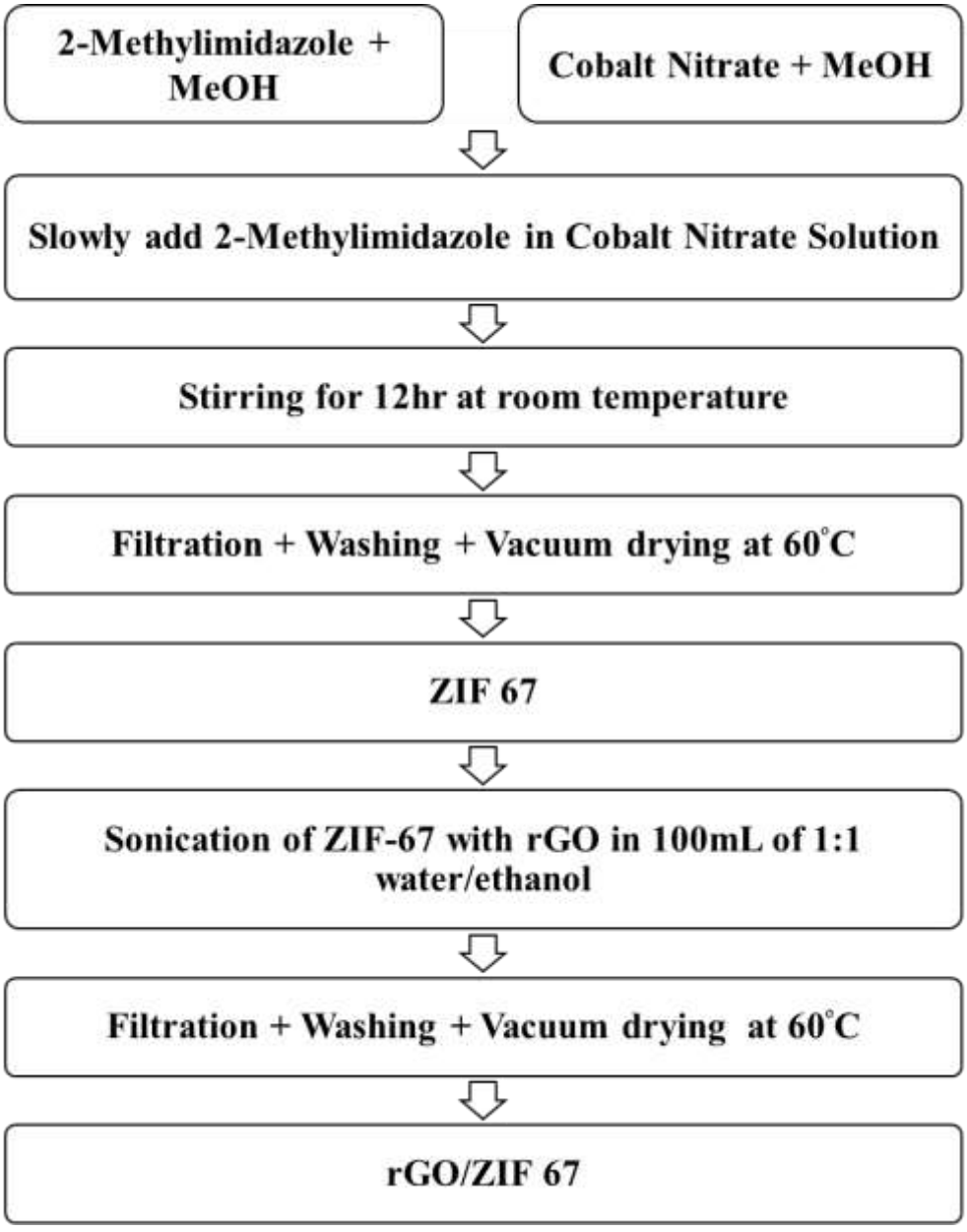

Figure 18: Scheme of ZIF-67 and rGO/ ZIF-67 Synthesis

3.7 Synthesis of Ni-MOF and rGO/Ni-MOF Composite

Material: Triethylamine (TEA), Nickel nitrate hexahydrate, benzene dicarboxylixacid (BDC), N,N-dimethylformamide (DMF). All these chemicals were used as per received.

a) Synthesis of Ni-BDC-MOF

Ni-BDC-MOF and rGO/Ni-BDC-MOF were prepared via hydrothermal method [109]. 2.72g of BDC and 2.95g of hydrated nickel nitrate in 250 ml of DMF stirred for 2hr. Next, 5ml of TEA was added drops wise. The solution was stirred until a complete suspension is formed (called reactants solution). The uniform solution autoclaved at 120°C for 12h. The sequence of all the steps involved in the synthesis of Ni-BDC-MOF is also explained in figure 19.

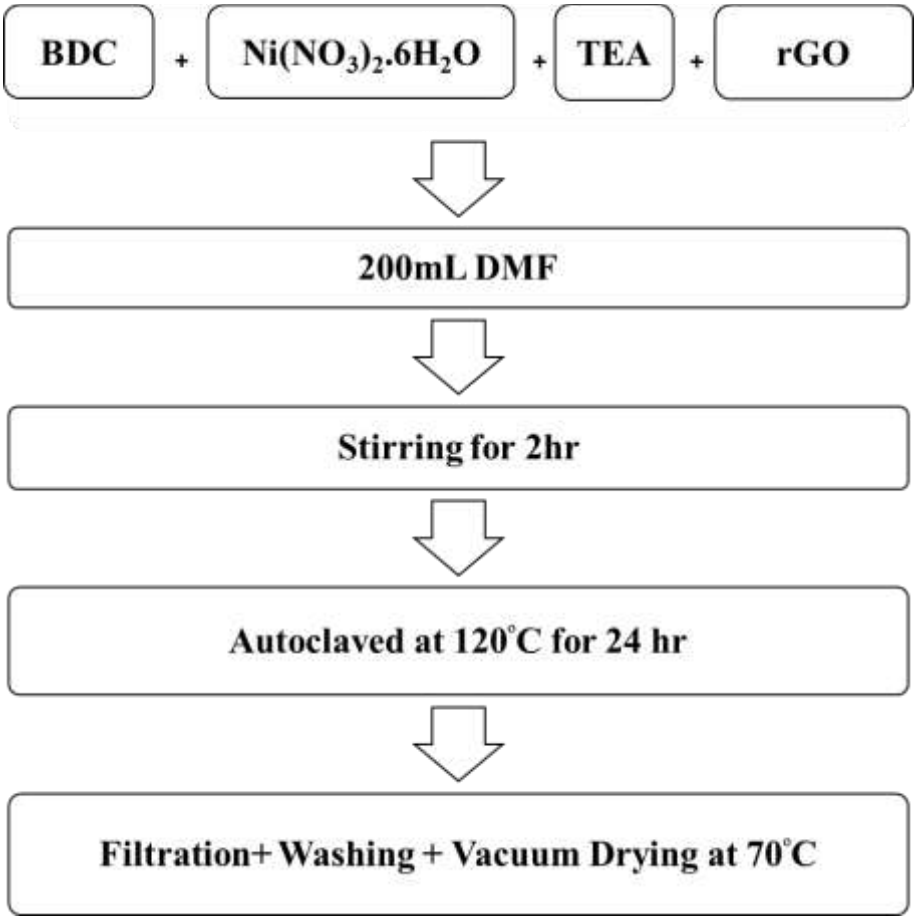

Figure 19: Scheme of rGO/Ni-BDC-MOF Synthesis

b) Synthesis of rGO/Ni-BDC-MOF Composite

For the synthesis of rGO/Ni-BDC-MOF composite reactants solution was prepared as explained above. After that GO added in reactants solution and sonicated for 1h. The

uniform solution autoclaved at 120°C for 12h. The sequence of all the steps involved in synthesis of composites of rGO/Ni-BDC-MOF is elaborated in figure 19.

3.8 Sensor Fabrication

Copper deposited PVC board was brought from local market and cut into suitable size. The circuit pattern drawn on it by lithography. In next step the resulted chip was dipped into $FeCl_3$ aqueous hot solution, which result in the removal of extra copper and copper integrated electrode (IE) was obtained.

The resulting products (rGO, N-doped rGO, rGO/ZIF and more) were compressed using a hydraulic press at a constant pressure to get thin pellets of sensing material. The pallet was placed on IE with help of an organic binder to get sensor.

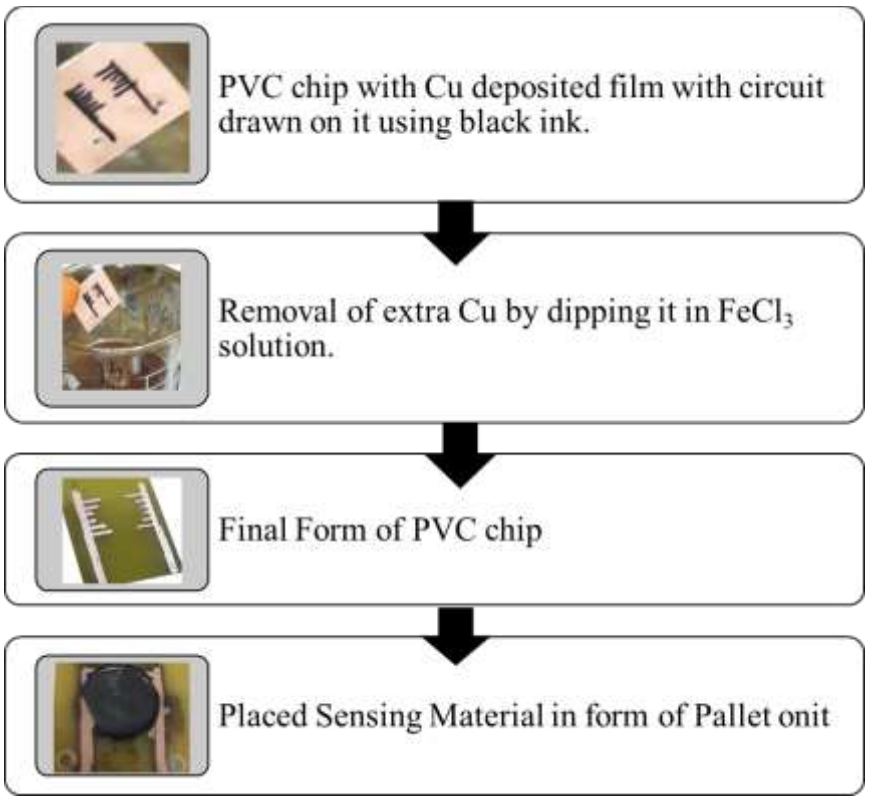

Figure 20: Schematic representation of Sensor Fabrication

3.9 Characterization

Synthesized materials characterized by following characterization techniques.

3.9.1. XRD Analysis

XRD is a feasible method to determine crystal dimensions. In this technique, diffraction of X-rays from different planes recorded and a diffraction pattern is

obtained following Braggs equation. In diffraction pattern the intensity depend on numbers of X-ray diffracted at particular angle 2θ, current and voltage of X-ray source. The position of peak in pattern defines the crystal configuration and helps to identify material [116]. Figure 21 describes the working principle of XRD equipment.

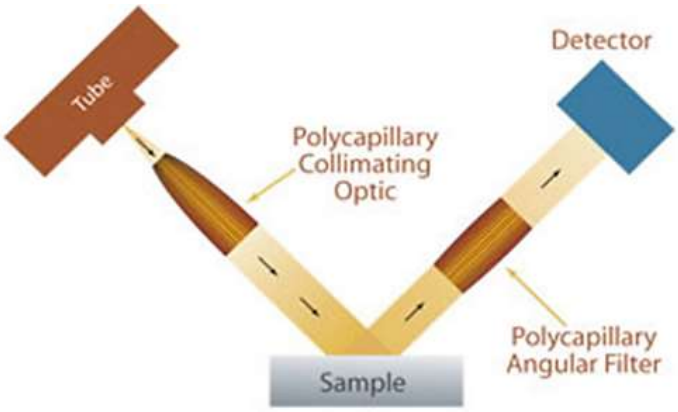

Figure 21: Working principle of XRD Machine

In this work, Powder XRD graphs were acquired from JSX 3201, Jeol, having radiation source of Cu Kα (λ=0.154059 nm) operated at 20 kV and 5 mA.

3.9.2. SEM Analysis

SEM is the mostly utilized for studying morphology, composition and minuscule details of the materials. In SEM high energy electrons beam is positioned on specimen's surface. The backscattered electrons in combination with secondary electrons form image. Backscattering electrons gives phase discrimination of material and secondary electrons gives information about topography and morphology. With the collision of electrons with sample atomic electrons X-rays formation takes place as well [117]. The working of SEM machine is explained in the figure 22.

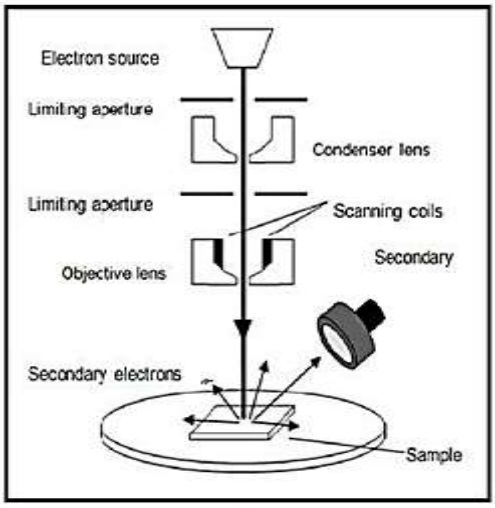

Figure 22: Working Principle of SEM Machine

In this research, SEM images were acquired from JEOL-JSM-6490A Japan, operated at 20 kV. Before SEM analysis, 250Å gold coating was done by Ion Sputter Coater model JFC-1500 make of JEOL, Japan.

3.9.3. FTIR Analysis

IR is a vibrational spectroscopy used to recognize type of functional groups and type of bonds present in a material. The Fourier Transformation (a mathematical procedure) is applied to get spectrum.

The covalent bonds are not rigid and keep in vibrational motion either stretching or bending. Absorption of infrared radiations change the state of vibration of bonds and produce a spectrum. This graph of spectrum is between percentage transmittance and wavenumber. The spectrum produce distinctive fingerprint of sample and these fingerprints helps to identify the functional groups present in the material [118].

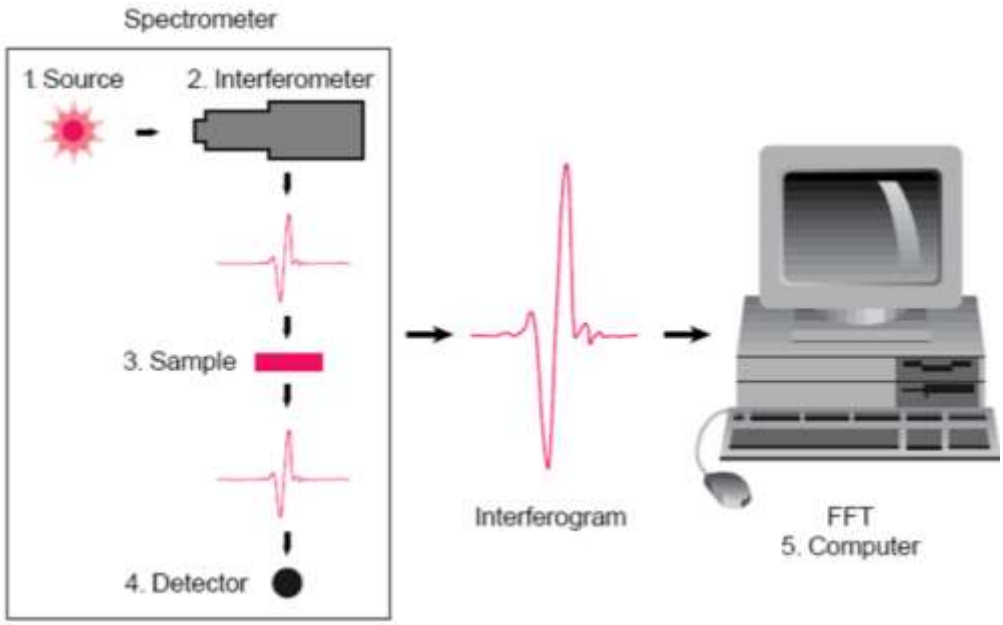

Figure 23: Working Principle of FTIR Machine

FTIR spectra obtained from Perkin Spectrum 100. FTIR spectroscopy is carried out by placing sample with in KBr pellets (10mm diameter). Approximately 1.0 % of sample is mixed into 200 mg of KBr powder and shaped in form of pellet. About 10 tons of force was applied under a vacuum for one minutes. After force was removed and a transparent pellet placed in equipment and analyzed in 4000 – 400 cm^{-1} range.

Chapter 4

Results and Discussions

4.1 XRD Analysis Results

Prepared materials was characterized using XRD, performed using JSX 3201, Jeol, Japan.

4.1.1. XRD Results of GO

XRD graph of GO is given in Figure 24. XRD analysis of GO confirms the Graphite oxidation and exfoliation. Pure graphite gives diffraction peak at 2θ =26˚ and after its oxidation the peak is shifted to 2θ =10˚ [111]. If there is any unreacted graphite in GO, it gives a minor peak at 2θ =26˚ along with peak at 10˚.As figure 24 illustrate that there is no peak at 26˚, which means that graphite is completely oxidized.

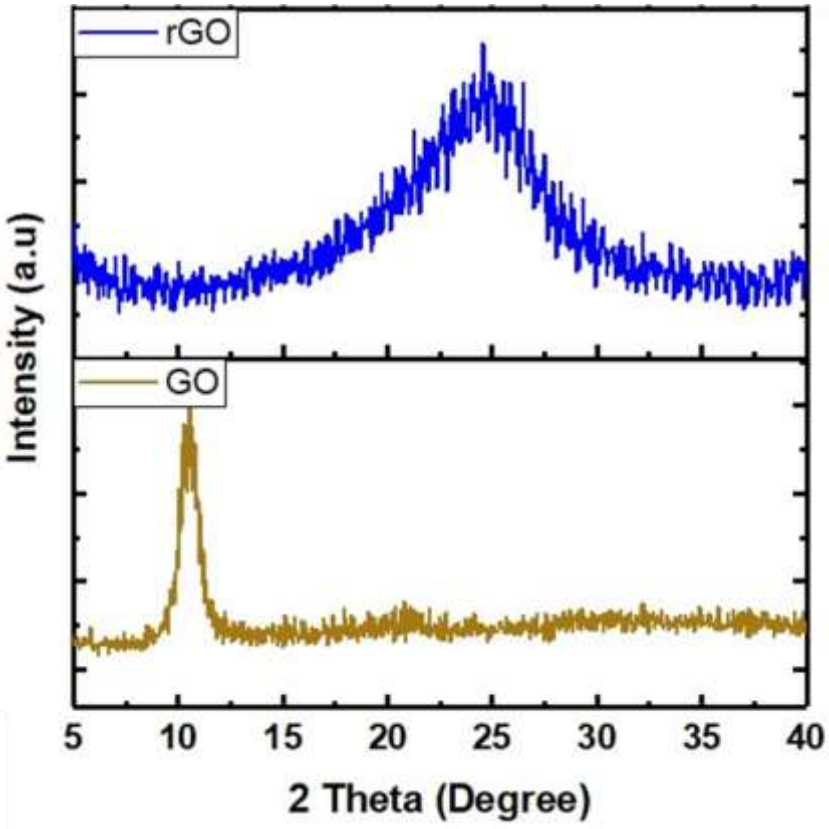

Figure 24: XRD Plot of GO and rGO

4.1.2. XRD Results of rGO

XRD pattern of rGO is given in Figure 24. The reduction of GO removes functional groups that increase the interlayer distance of Graphite layers and reduce the stacking

to single layer to few layers. The XRD graph presented in figure 25 describe this phenomena. The characteristic peak of GO at **2θ=10º** completely vanished after reduction and a wide diffraction peak at **26º** is appeared which endorse the formation of rGO [119]. The broadening is because of low order of stacking.

4.1.3. XRD Results of N-doped rGO

The XRD graph of N-doped rGO is shown in figure 25. After heating GO with NH_4NO_3 at 350°C in muffle furnace, the XRD pattern become similar to rGO. This corresponds to a reduction of GO while nitrogen doping.

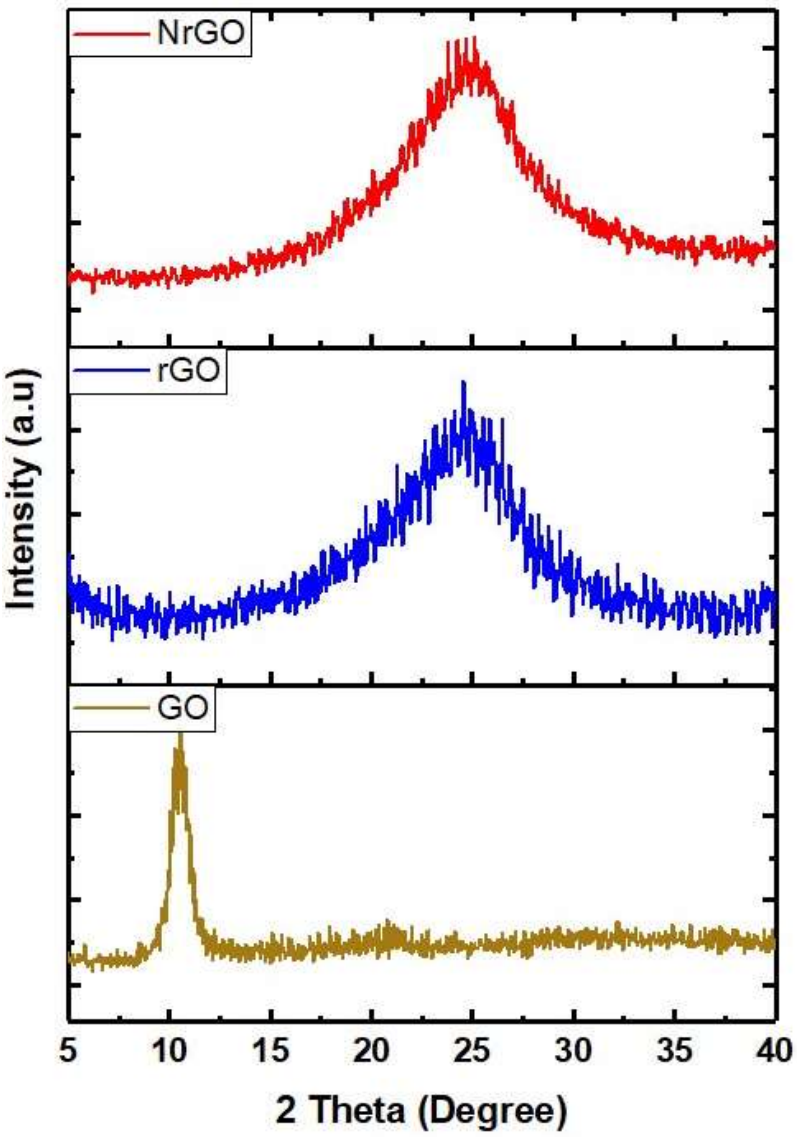

Figure 25: XRD Plot of Nitrogen Doped rGO

If we compare it with XRD pattern of GO we can see that characteristic peak of GO at **2θ=10º** completely vanished in XRD pattern of NrGO.

4.1.4. XRD Results of Fe_3O_4 Nanoparticles and rGO/ Fe_3O_4

Figure 26 demonstrate the XRD graph of the iron nanoparticles and it's composite with rGO. Figure 26a, shows the diffraction peaks of iron oxide according to standard JCPDS card (PDF # 87-2334), it can be seen that Fe_3O_4 particles are well-crystallized with high purity.

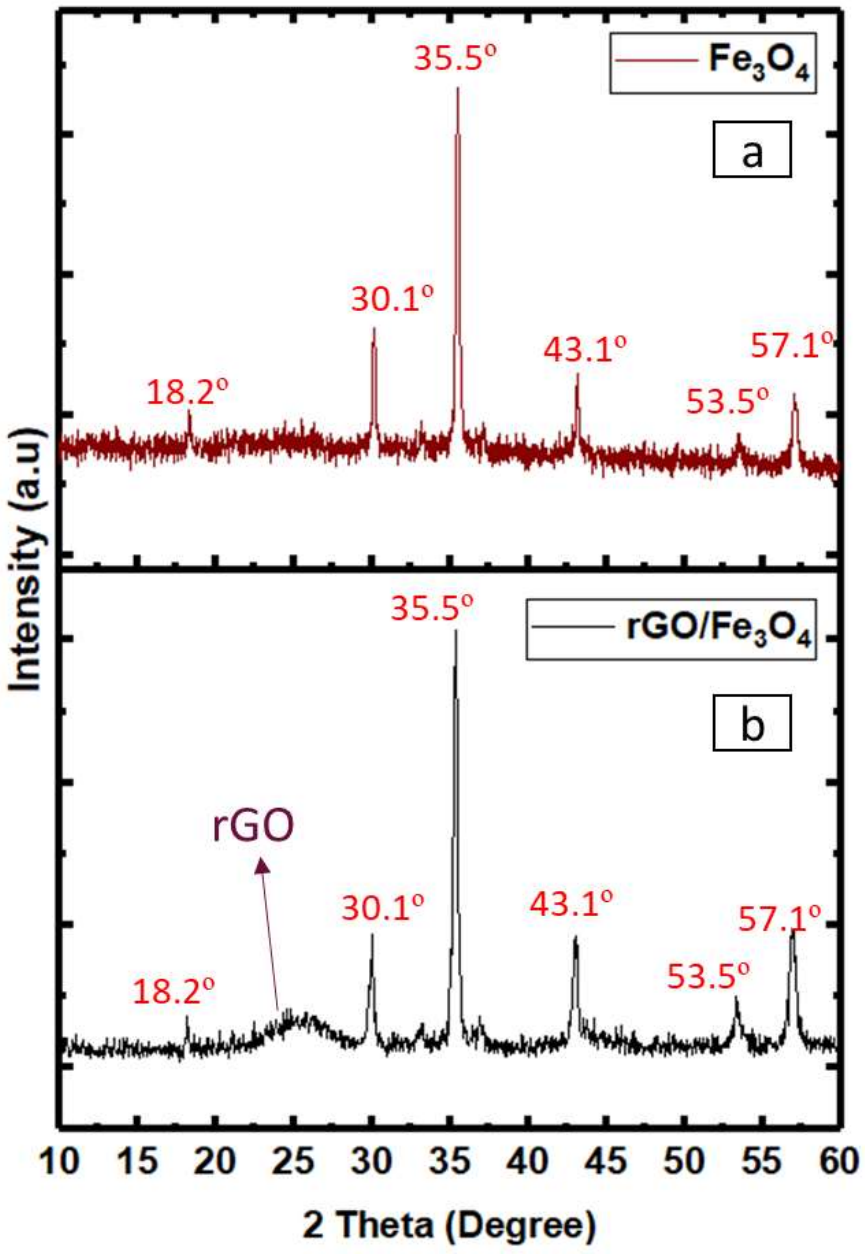

Figure 26: (a) XRD Plot of Fe_3O_4 Nanoparticles

(b) XRD Plot of rGO/ Fe_3O_4 Composite

However, in figure 26b other than the sharp diffraction peaks of Fe_3O_4, another wide peak of rGO at 26° is present, which shows that rGO and Fe_3O_4 nanoparticles are homogenously combined.

4.1.5. XRD Results of CoOOH and rGO/ CoOOH Composite

XRD graph of the CoOOH is given Figure 27 with and without rGO in range of 2θ=10–60º. Figure 27a, illustrate the XRD graph of CoOOH and comparison with JCPDS card No. 26-0480 confirms the synthesis of CoOOH particles [24].

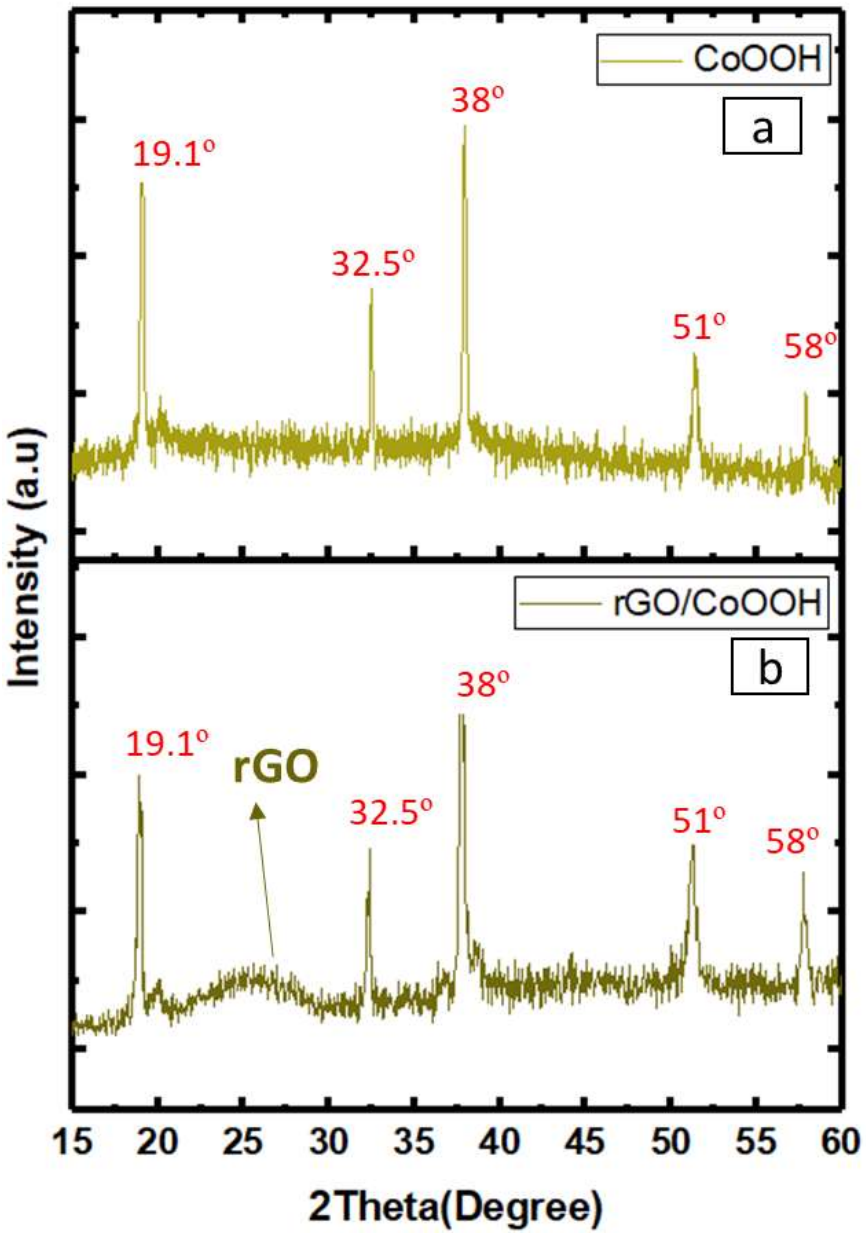

Figure 27: (a) XRD Plot of CoOOH Nanoparticles

(b) XRD Plot of rGO/CoOOH Composite

However, in figure 27b other than the peaks of CoOOH another wide peak of rGO at 26° can be witnessed which shows that rGO and CoOOH nanoparticles are homogenously combined.

4.1.6. XRD Results of ZIF-67 and rGO/ ZIF-67 Composite

Figure 28 demonstrate the XRD graph of the ZIF-67 and rGO/ZIF-67 composite. XRD of results of synthesis ZIF-67 are shown in figure 28a is in harmony with the Zhou et al. XRD pattern [74]. The dominant peaks at 2θ= 7.2°, 10.28°, 12.56°, 14.48°, 16.32°, 17.92°, 22.6°, 24.36° shows crystals phase purity and rhombic structure.

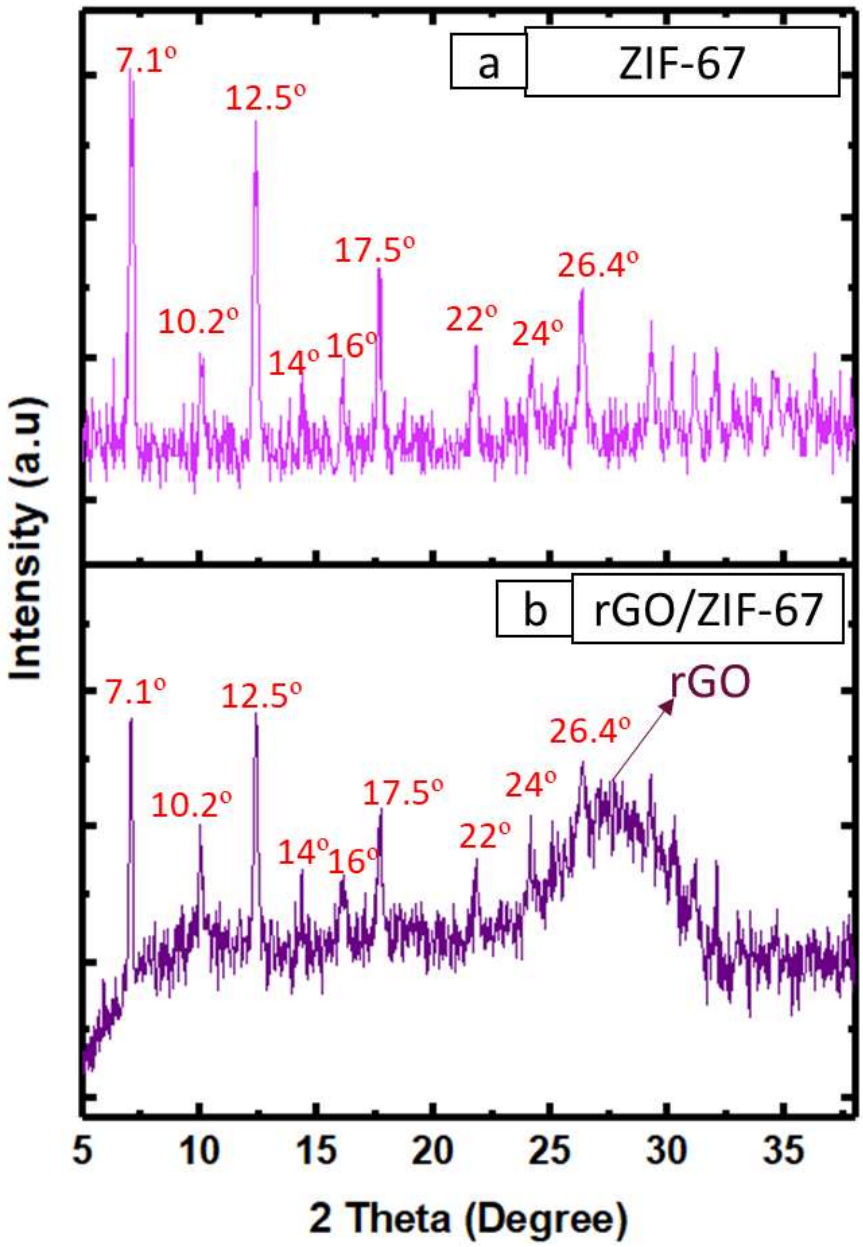

Figure 28: (a) XRD Plot of ZIF-67

(b) XRD Plot of rGO/ ZIF-67 Composite

Figure 28b show the XRD pattern of rGO/ZIF-67, it can be observed that other than the peaks of ZIF67, a broad peak of rGO at 26° can be seen which confirms that the combination of rGO with ZIF-67.

4.1.7. XRD Results of Ni-BDC and rGO/Ni-BDC Composite

Figure 29 demonstrate the XRD graph of Ni-BDC-MOF and rGO/Ni-BDC composite. Synthesized Ni-BDC-MOF XRD result is presented in figure 29a. The dominant peaks at 2θ= 9.5°shows crystals phase purity and sheet structure of MOF.

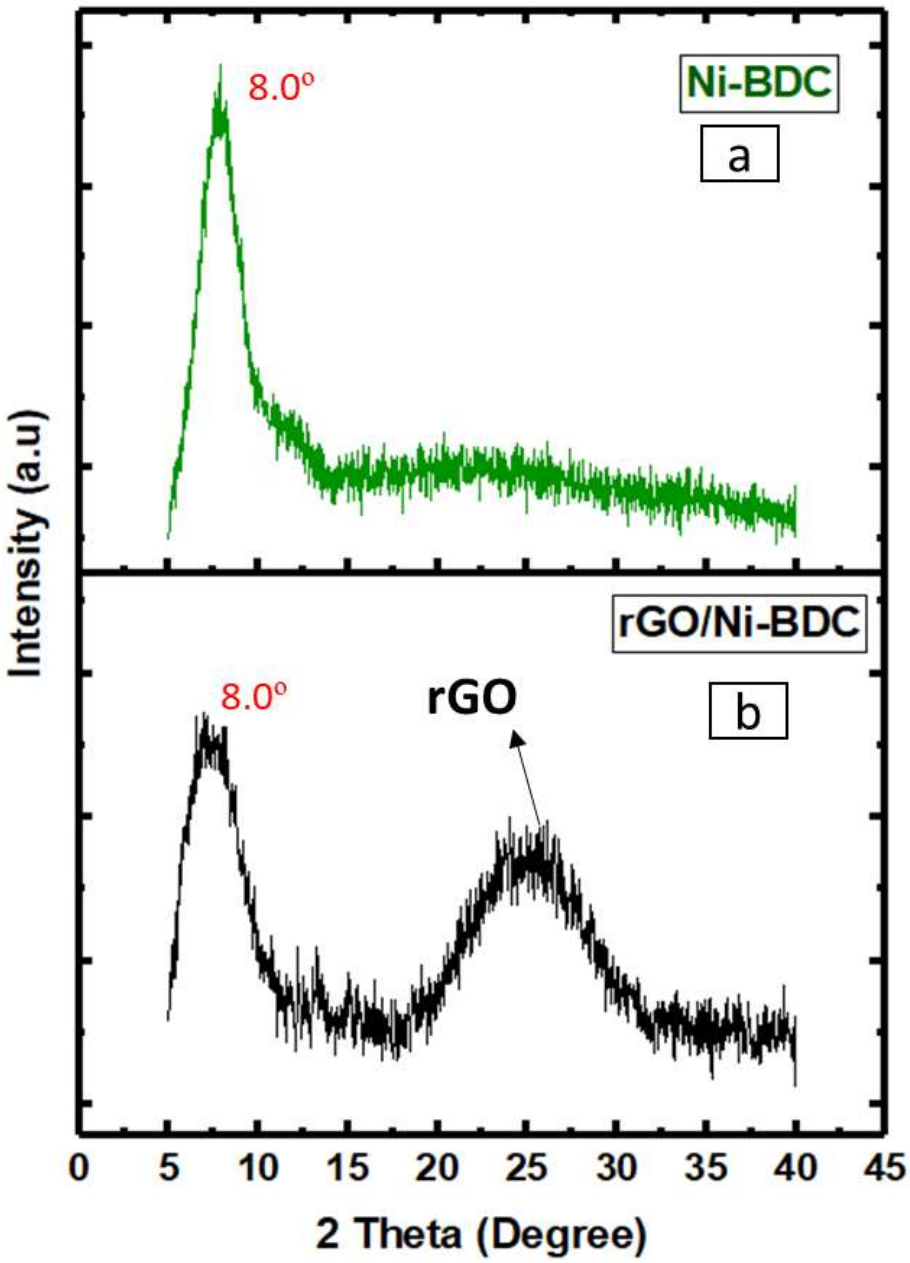

Figure 29: (a) XRD Plot of Ni-BDC-MOF

(b) XRD Plot of rGO/ Ni-BDC-MOF Composite

Figure 29b show the XRD pattern of rGO/Ni-BDC-MOF, it can be detected that other than the peak of Ni-BDC a broad peak of rGO at 26° can be observed in their XRD graph which confirms that the combination of rGO with Ni-BDC-MOF.

4.2 SEM Analysis Results

SEM of prepared materials carried using JEOL-JSM-6490A Japan operating at 20kv.

4.2.1. SEM Analysis of GO

SEM image of GO in figure 30 illustrate that GO has a 2D sheet-like structure, GO sheets has lamellar configuration with distinguished edges.

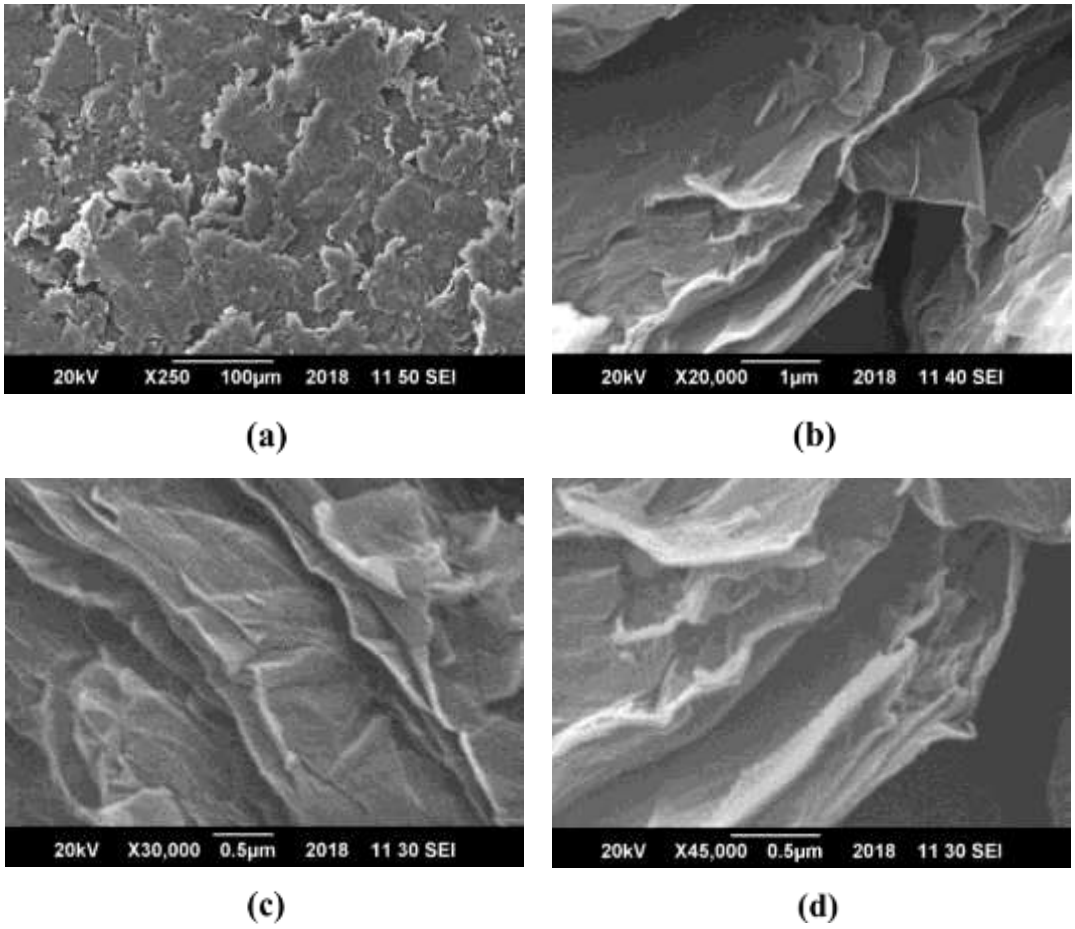

Figure 30: SEM Pictures of GO

Moreover, GO sheets are thicker at the edges because functional groups are majorly present at the edges.

4.2.2. SEM Analysis of rGO

SEM pictures of rGO are shown in figure 31. Images reveals that free floating rGO nano-sheets are single or few-layered with 2D membrane like structure and sheets are entangled with each other. Sheets have wrinkled and rippled structure because of exfoliation and restacking processes.

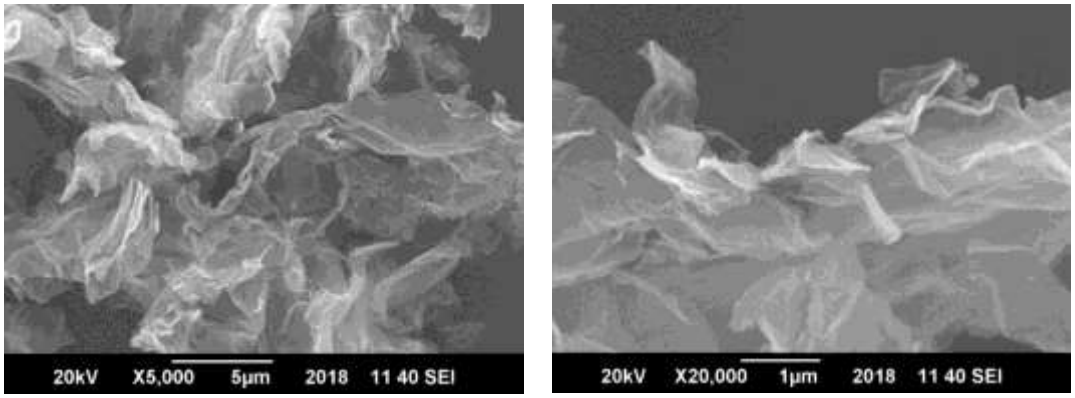

Figure 31: SEM Pictures of rGO

4.2.3. SEM Analysis of N-doped rGO

SEM pictures of N-doped rGO are shown in figure 32. Images reveals that exfoliated layers of nitrogen doped rGO are similar to rGO.

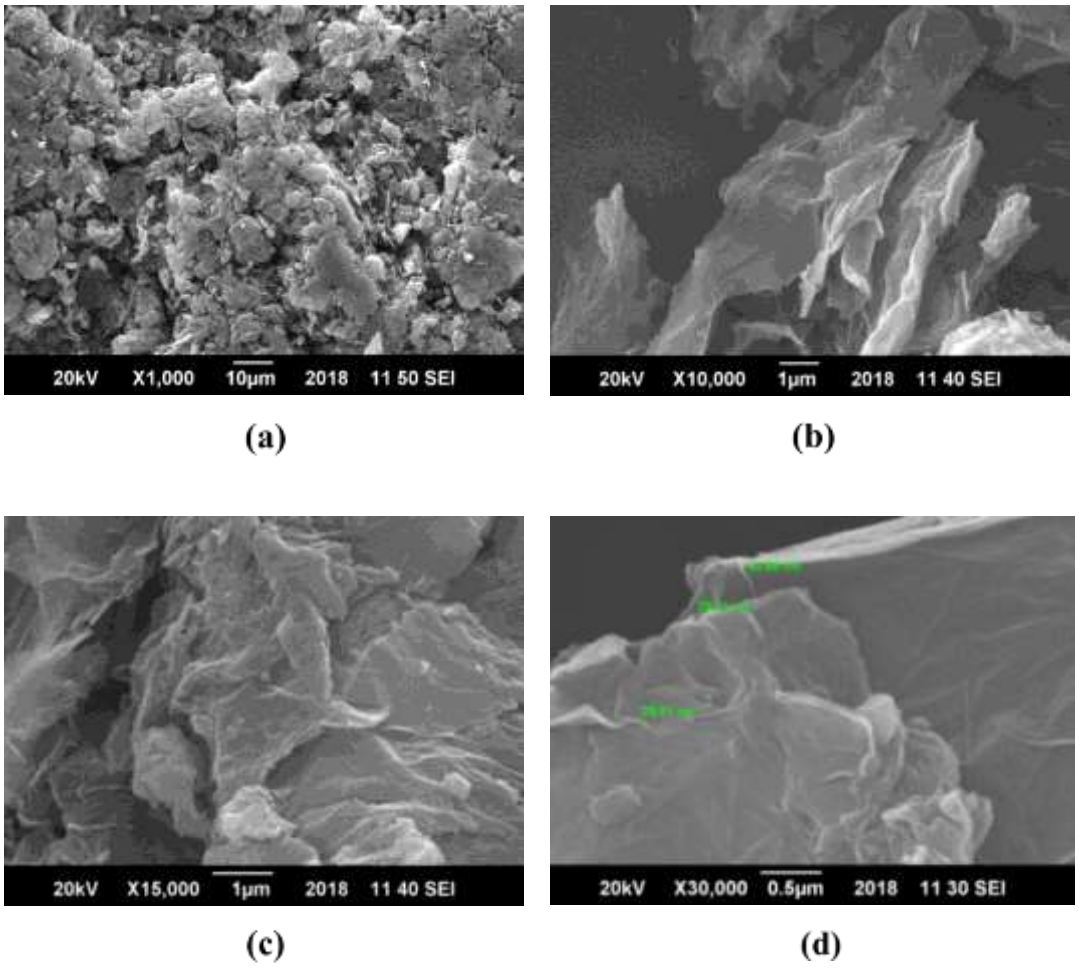

Figure 32: SEM Pictures of N-doped rGO

However, exfoliated sheets are less aggregation than rGO. The sheet thickness is about 33nm with 2D structure. The crumpled nature created due to the defects formed during the exfoliation and heteroatom doping reaction.

4.2.4. SEM Analysis of Fe_3O_4 and rGO/ Fe_3O_4 Composite

SEM pictures of Fe_3O_4 Nanoparticles and rGO/ Fe_3O_4 Composite are shown in figure 33. Figure 33a illustrate the SEM analysis of Fe_3O_4, as image illustrate that Fe_3O_4 particles are uniform and spherical in shape with size ranging from 250 nm to 350 nm.

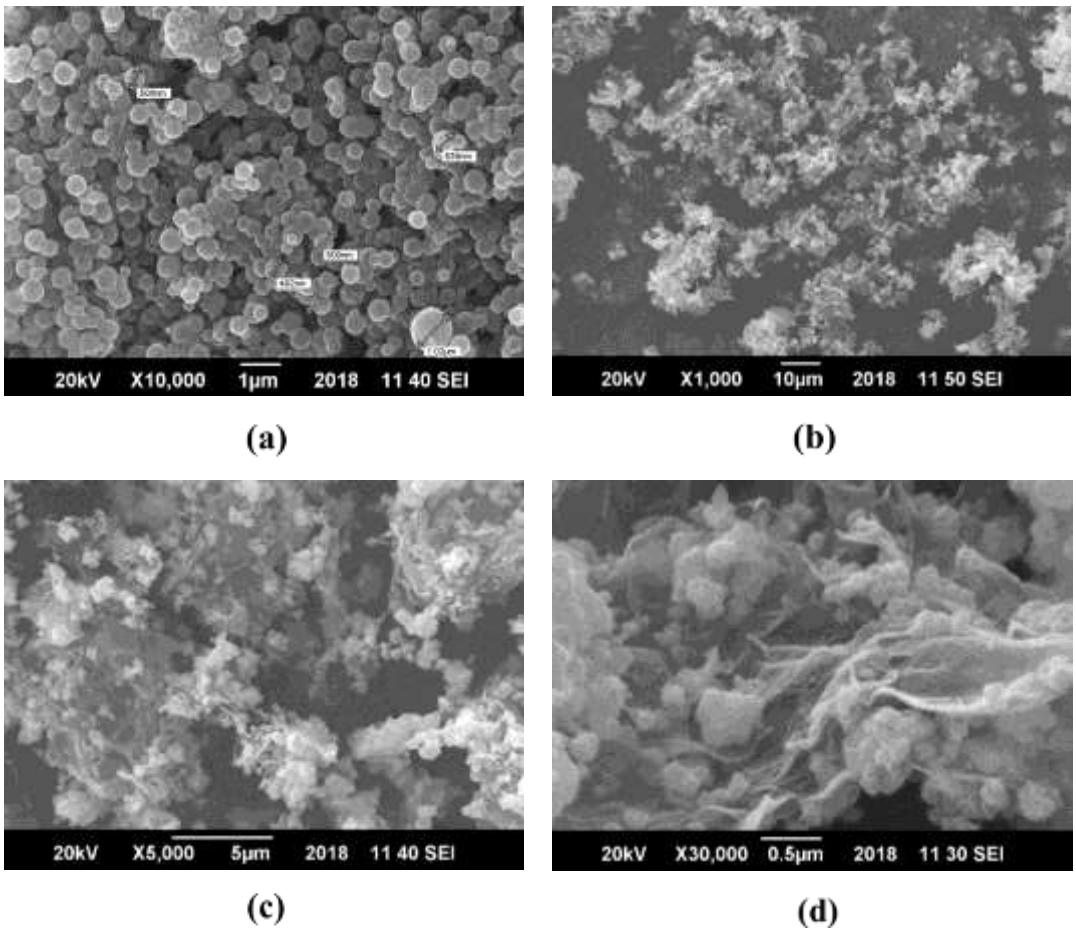

Figure 33: (a) SEM Picture of Fe_3O_4 Nanoparticles

(b-c) SEM Images of rGO/ Fe_3O_4 Composite

Figure 33(b-d) exhibits morphology of rGO/ Fe_3O_4 composite, as images show Fe_3O_4 particles are uniformly embedded on rGO sheets. Additionally, Fe_3O_4 microspheres have rough surface which increase their adhesion to the rGO sheets.

4.2.5. SEM Analysis of CoOOH Nanoparticles and rGO/CoOOH Composite

The SEM analysis of CoOOH Nanoparticles and rGO/ CoOOH composite is given in figure 34. Figure 34(a-b) explained the SEM analysis of pure CoOOH, as image

illustrate that CoOOH particles have spongy morphology. Figure 34(c-d) exhibits morphology of rGO/CoOOH composite, as images shows CoOOH particles are uniformly embedded on the rGO sheets.

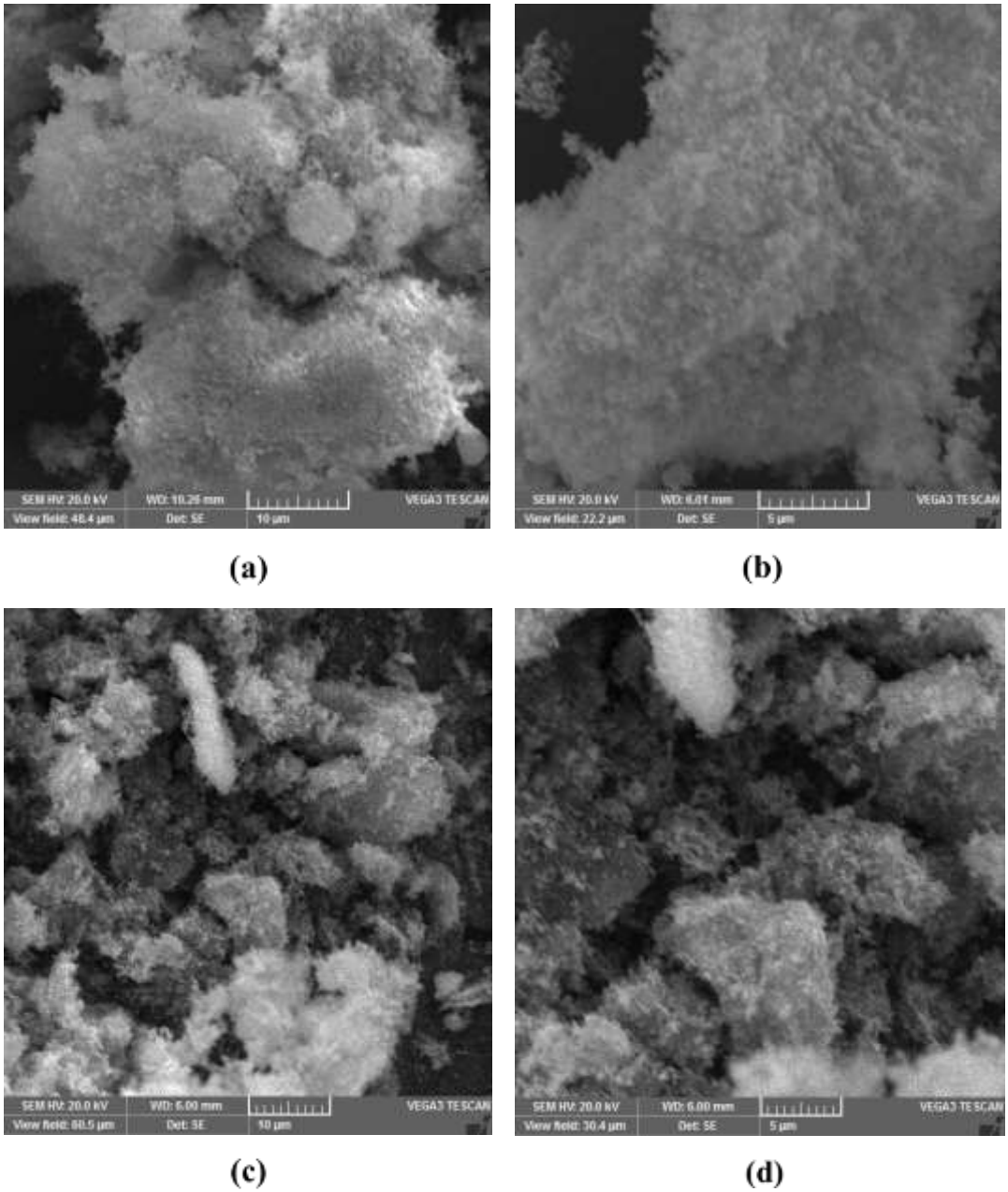

Figure 34: (a-b) SEM Picture of CoOOH Nanoparticles

(c-d) SEM Picture of rGO/ CoOOH Composite

4.2.6. SEM Analysis of ZIF-67 and rGO/ZIF-67 Composite

The SEM pictures of ZIF-67 its composite with rGO is shown in figure 35. SEM images 35(a-b) displays the morphology of pure ZIF-67, as image illustrate that nano-sized crystals ZIF-67 have rhombic dodecahedrons structure with size ranging from

150-400 nm.[120] SEM images 35(c-f) are of rGO/ZIF-67composite, images indicates the homogeneous dispersal of ZIF-67 on graphene sheets.

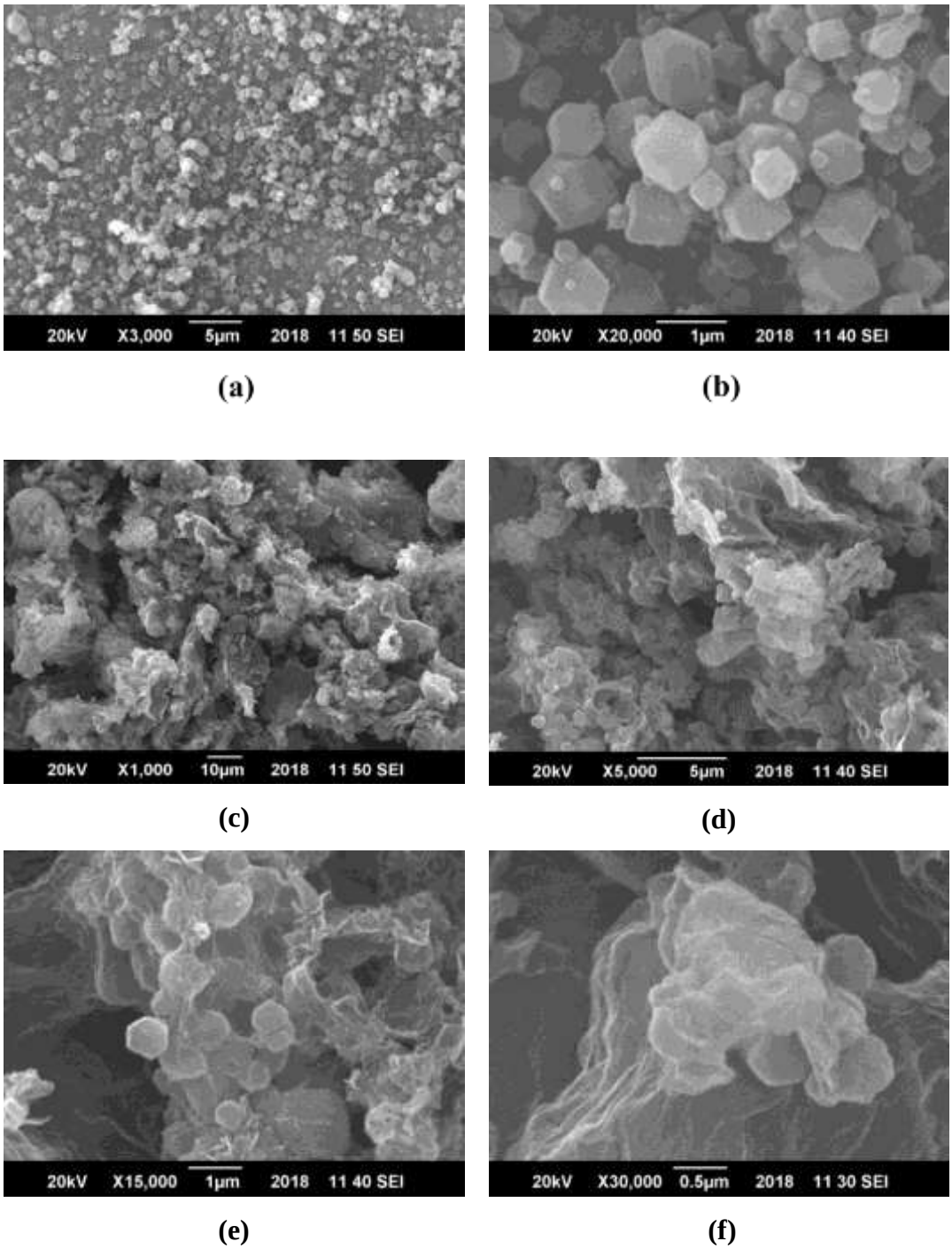

Figure 35: (a-b) SEM Pictures of ZIF-67

(c-f) SEM Pictures of rGO/ ZIF-67 Composite

This distribution revamp the electric conductivity of ZIF-67 and make it suitable for chemi-resistive type gas sensor.

4.2.7. SEM Analysis of Ni-BDC and rGO/ Ni-BDC Composite

The scanning electron microscopy (SEM) pictures of Ni-BDC and rGO/Ni-BDC composite is given in Figure 36. Figure 36(a-b) illustrates the morphology of Ni-BDC-MOF it can be seen that the MOF have a sheet morphology. Figure 36(c-d) shows morphology of rGO/Ni-BDC-MOF composite, it can be seen that Ni-MOF sheets are homogenously attached with rGO sheets.

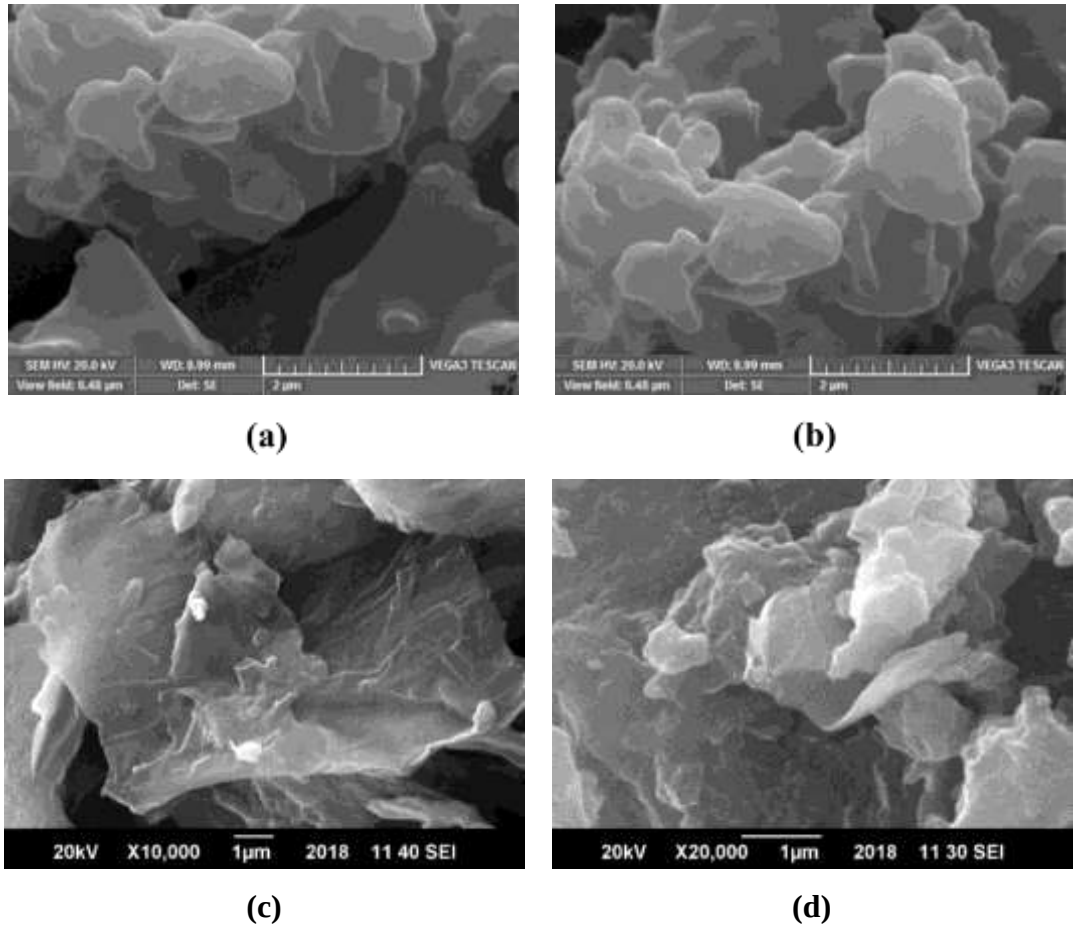

Figure 36: (a-b) SEM Pictures of Ni-BDC

(c-d) SEM Pictures of rGO/ Ni-BDC Composite

4.3 FTIR Analysis Results

FTIR analysis of prepared materials was carried out using Perkin Spectrum 100.

4.3.1 FTIR Analysis of GO

When FTIR performed on GO showed in figure 37. Following groups were found in IR spectra which confirmed the oxidation of graphite.

- O-H at 3420 cm^{-1}
- C=O at 1700-1740cm^{-1}
- C=C bonds (1590-1620 cm^{-1})
- C-O at1250 cm^{-1}

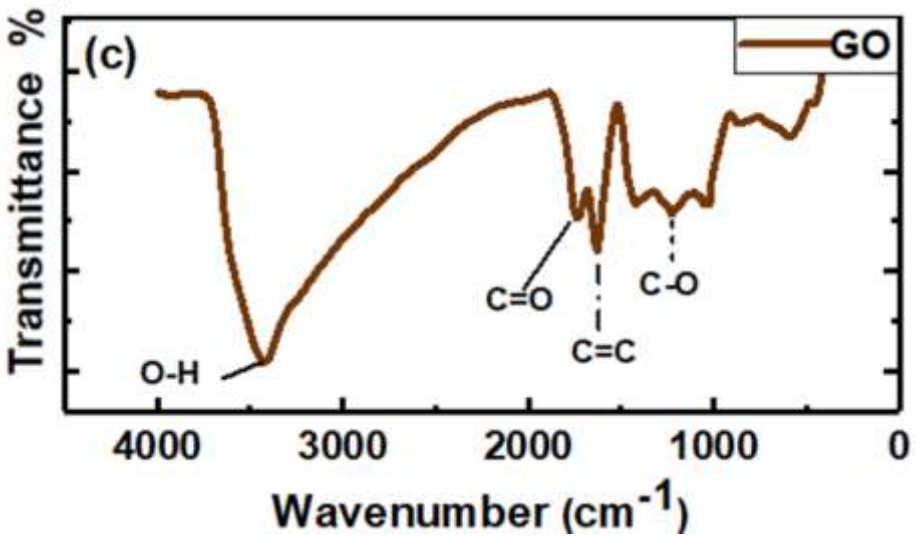

Figure 37: FTIR Plot of GO

4.1.16. FTIR Analysis of rGO

Reduction removes the functional groups attached to the planes of GO and this can be seen in FTIR pattern of rGO as shown in figure 38. If we compare GO and rGO FTIR spectrum it can be seen that reduction of GO have significantly reduced. carbonyl (-C=O), epoxy groups (C-OC) and hydroxyl (-OH) from the graphitic ring.

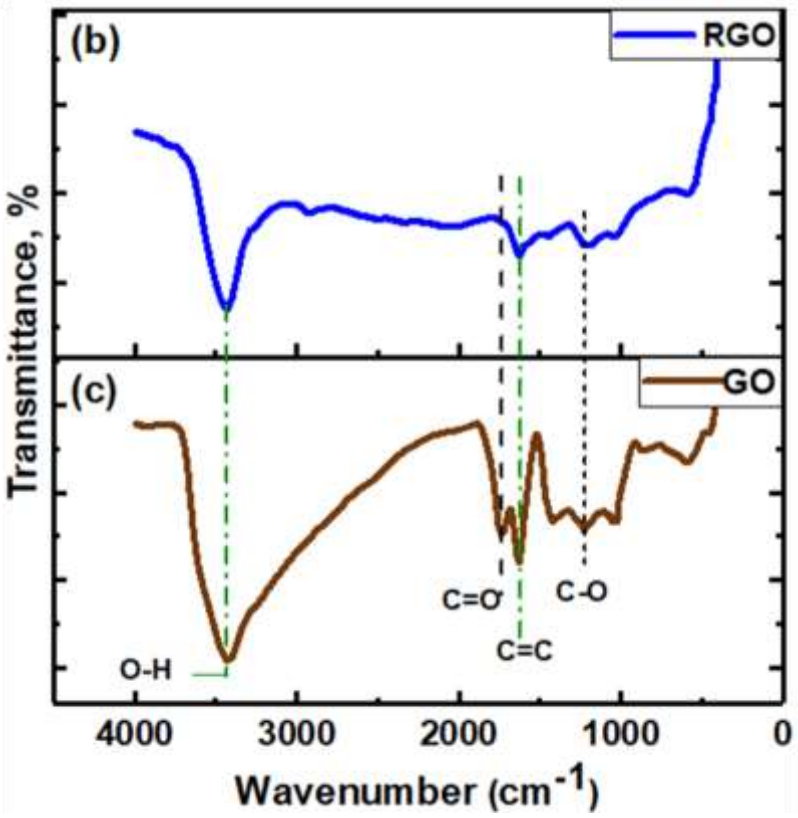

Figure 38: FTIR Plot of rGO

4.1.17. FTIR Analysis of N-doped rGO

FTIR spactra of N-doped rGO is given in figure 39. As compare to rGO, in FTIR pattern of Nitrogen Doped rGO have two addition peaks at 1180 cm^{-1} for Carbon single bond Nitrogen (C-N) and 1465 cm^{-1} band for C=N vibration along with C=C band which represents nitrogen doping in graphene ring.

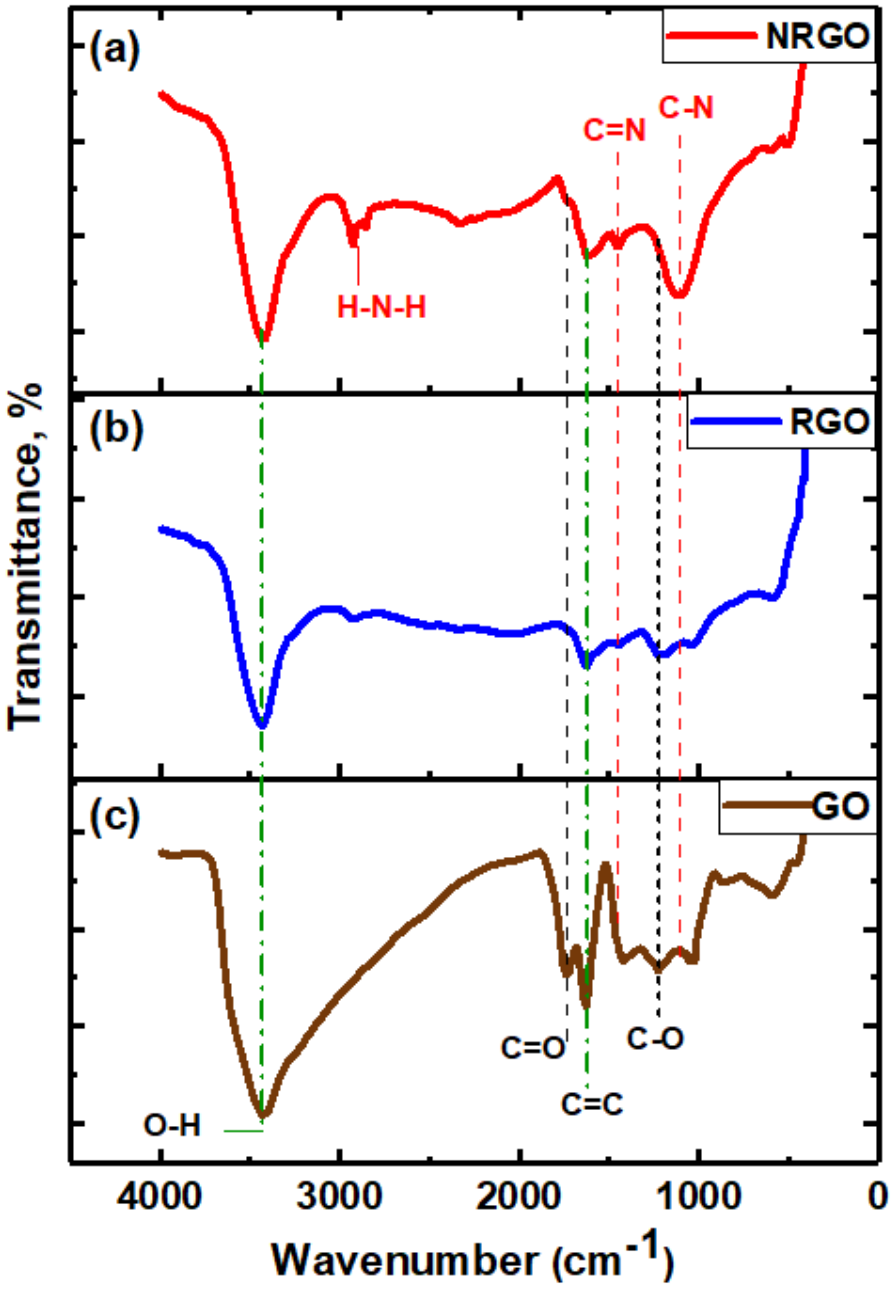

Figure 39: FTIR Plot of N-doped rGO

4.1.18. FTIR Analysis of CoOOH and rGO/ CoOOH Composite

FTIR analysis of CoOOH is given in Figure 40a. A large peak of O–H at 2900 cm^{-1} and 3400 cm^{-1} confirms the presence of -O-H. Peak at 3400 $cm^{-1}$is because of O–H

bonds which interacts with other nearby atoms. Two small peaks around 1600 cm^{-1} and around 1730 cm^{-1} shows the bonding of Co=O. A medium peaks at~580 cm^{-1} is due to $Co–O^{-2}$ complex in CoOOH.

FTIR analysis of rGO/CoOOH is given in Figure 40b. Other than the bands of CoOOH (O-H ~2900 cm^{-1} and~3400 cm^{-1} ,~1630 cm^{-1} and~1730 cm^{-1} of Co=O and ~580 cm^{-1}~ 670 cm^{-1} are of $Co–O^{-2}$ complex.) C-O peak and C=C is also appeared in FITR spectrum of rGO/CoOOH composite [121].

A noticeable change in O-H band at 3400cm^{-1} can be seen, this is because of the unremoved O-H group of rGO.

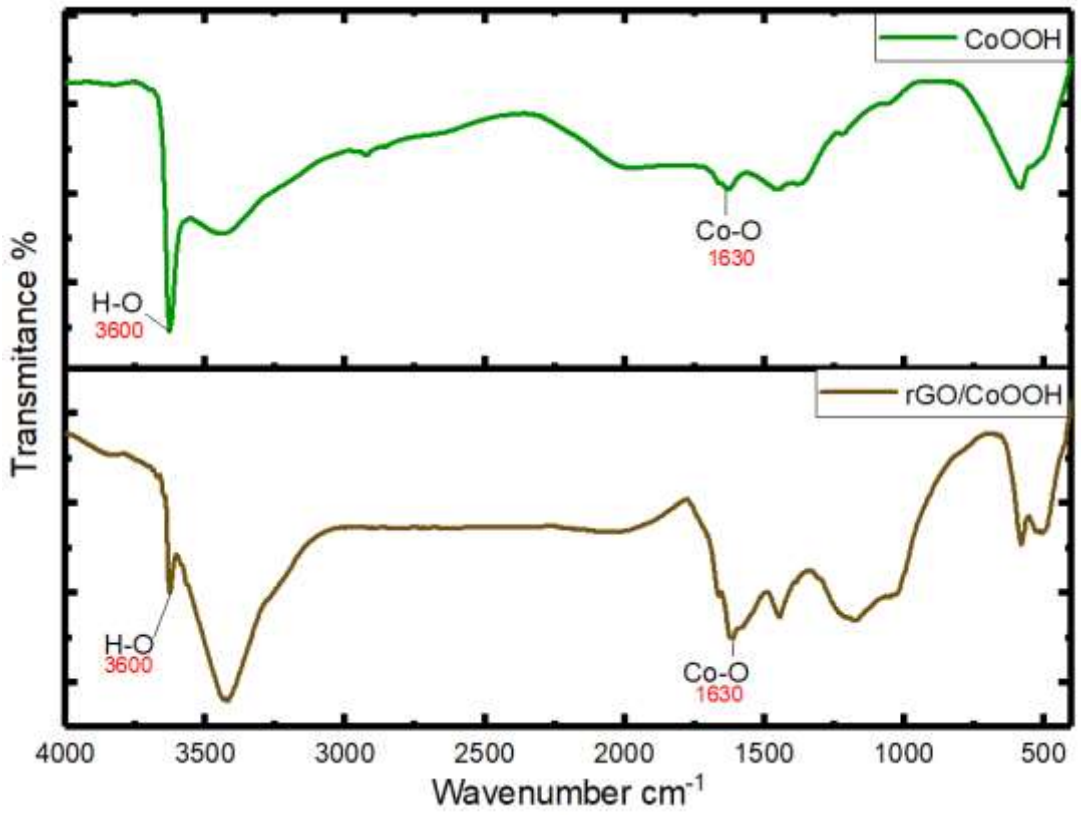

Figure 40: FTIR Plot of CoOOH and rGO/ CoOOH Composite

4.4 Sensors Response

Sensor response to varies concentration of CO was measured using a home-built system consisting of a closed chamber with sensor holder, gas source and Agilent Multi-meter. The test gas was generated according to desired concentration and allowed to enter in testing chamber. The setup is shown in figure 41.

The change in resistance with time was measured by multi-meter. The percentage response was calculated from given formula;

$$\%R = \frac{R_{gas} - R_{air}}{R_{air}} \times 100$$

Response of rGO, Nitrogen Doped rGO, rGO/Fe_3O_4, rGO/CoOOH, rGO/ZIF-67 was calculated at 1000, 2000, 3000, 4000 and 5000 ppm of CO and response curves are given in figure 4.21 to 4.24.

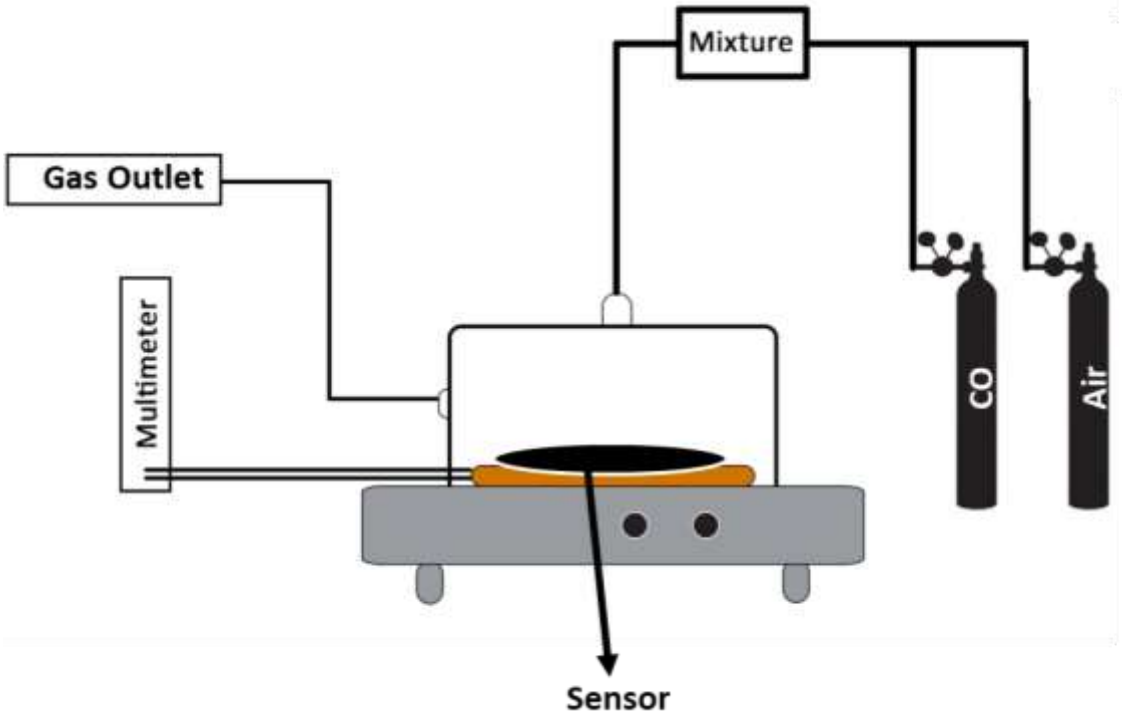

Figure 41: Response Measuring Setup.

4.4.1. Response of Nitrogen Doped Reduced Graphene Oxide

N-doped rGO Sensor show p-type behavior. Figure 42 show the response of N-doped rGO sensor towards 1000ppm level of CO. Dynamic response curve have three regions;

- Response region.
- Saturation region
- Recovery region.

As graph show sensor response rise with the escalation of CO gas level and reach to saturation plateau after saturation curves move to desorption mode which represent the recovery of sensor.

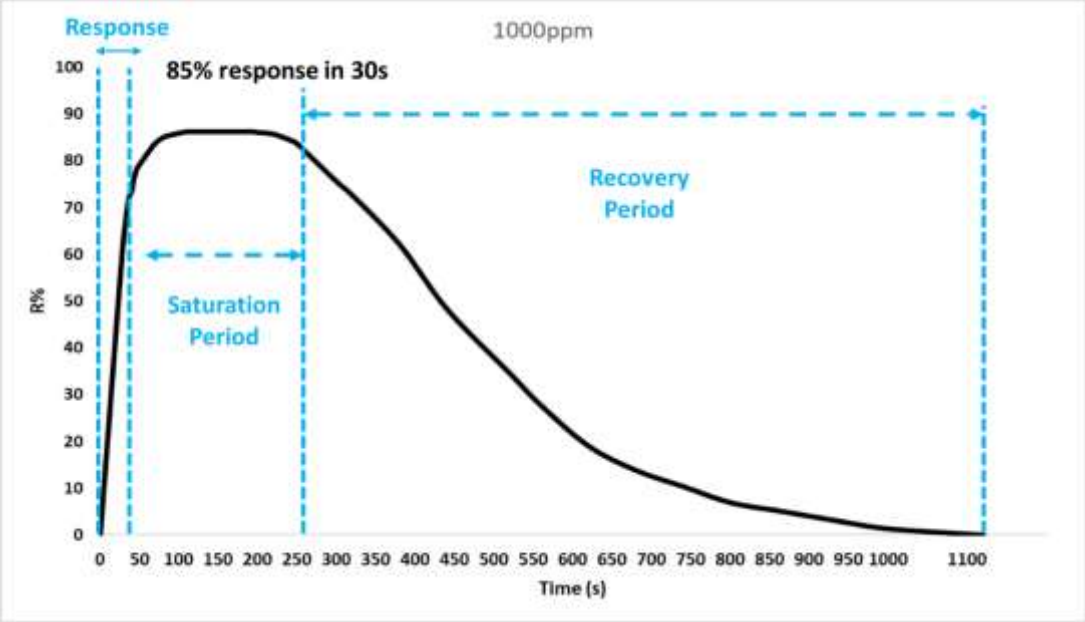

Figure 42: Dynamic Response Curve of N-doped rGO Sensor for 1000ppm of CO Level

Sensor show similar behavior against 2000-5000 ppm of CO exposure at room temperature (30^{o}C) and average response time of 30s as shown in figure 43.

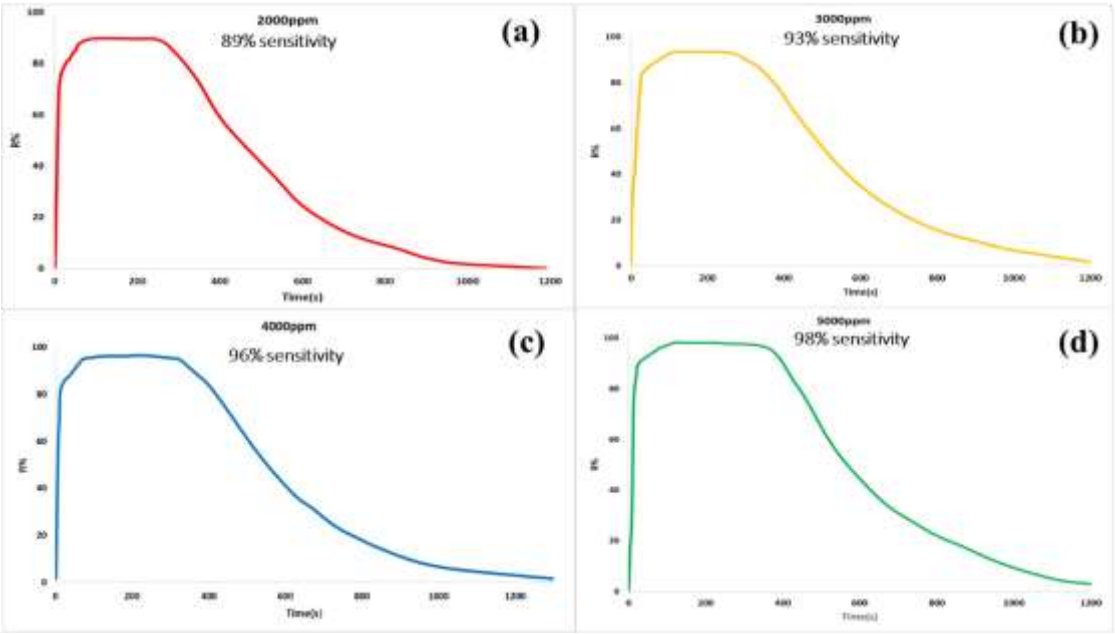

Figure 43: Dynamic Response Curves at Different CO Levels for N-doped rGO Sensor

By combining all the response curves as shown in figure 44, we can see that the percentage response increase with the increase in CO level.

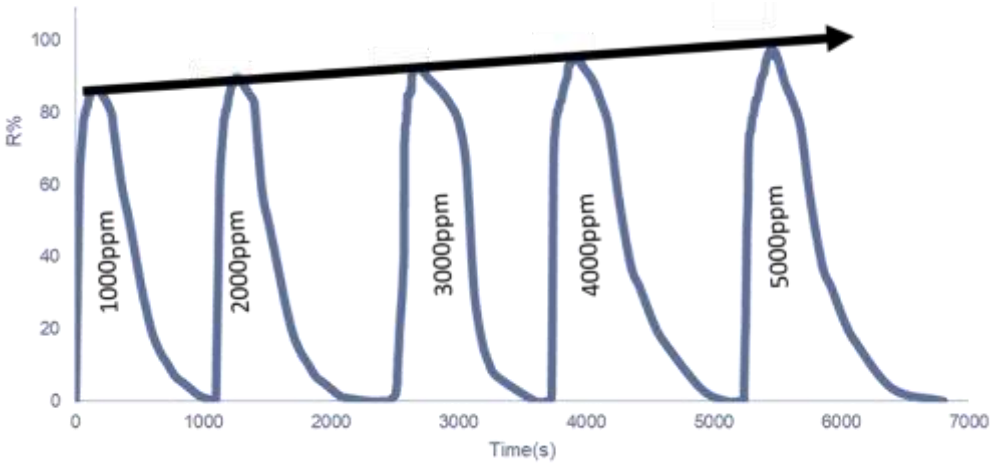

Figure 44: Combined Response curve of N-doped rGO Sensor

4.4.2. Response of rGO/Fe_3O_4

Fe_3O_4 nano-particles based sensor operates at the temperature above 200°C as reported by C.Hung, combination of Fe_3O_4 nano-particles with rGO did not significantly reduced its operation temperature.

4.4.3. Response of rGO/CoOOH

Ren-Jang [103] reported the CoOOH based CO sensor operates at 80°C. By combining CoOOH with rGO we successfully reduce its operating temperature to room temperature. Figure 45 depicts the sensing characteristics of rGO/CoOOH towards 1000ppm of CO.

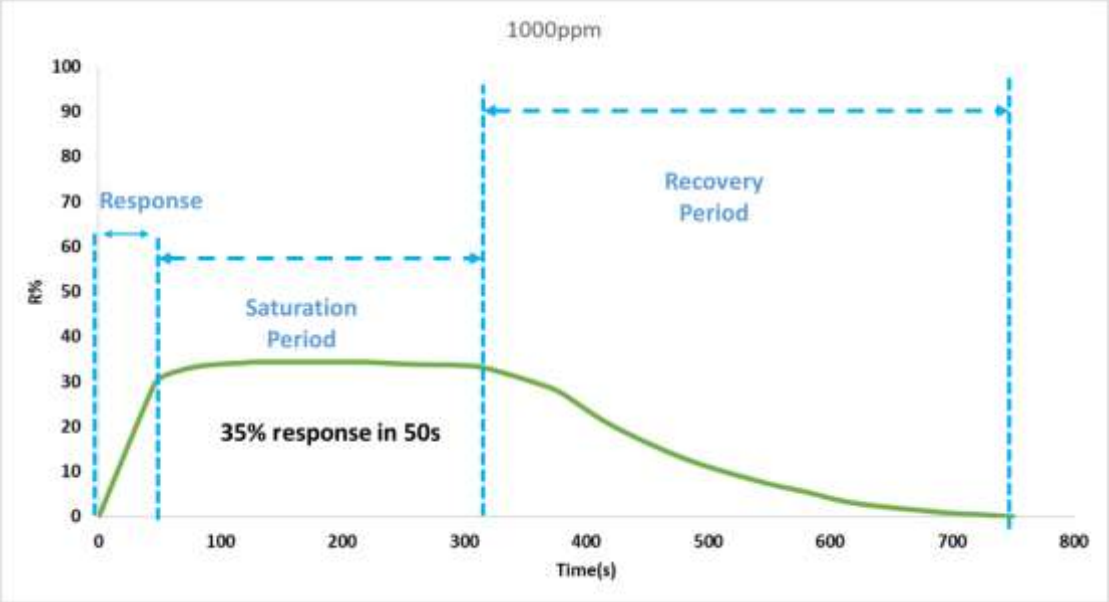

Figure 45: Dynamic Response Curve of rGO/CoOOH Sensor for 1000ppm of CO Level

Sensor show p-type behavior with 34% at 1000ppm, 38% at 2000ppm, 42% at 3000ppm, 45% at 4000ppm and 50% sensitivity against 5000 ppm of CO exposure at room temperature (30^{o}C) and average response time of 90s.

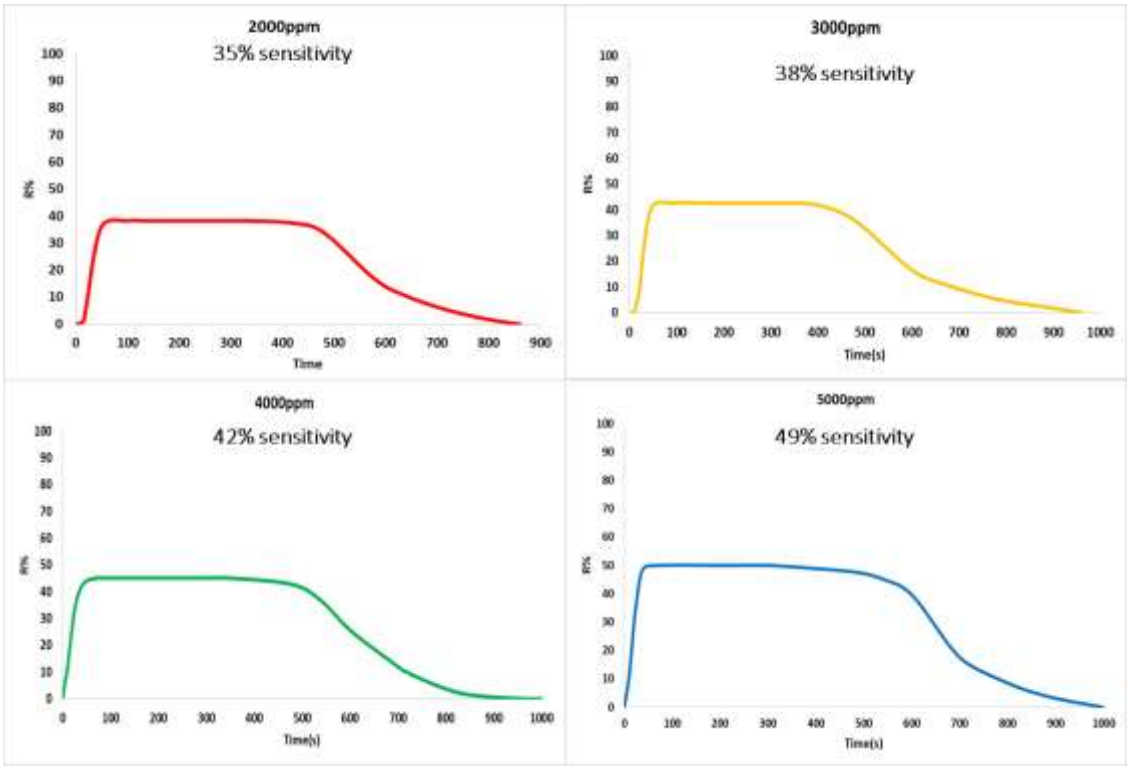

Figure 46: Dynamic Response Curves at Different CO Levels for rGO/CoOOH Sensor

By combining all the response curves as shown in figure 47 we can see that the percentage response increase with the increase in CO level.

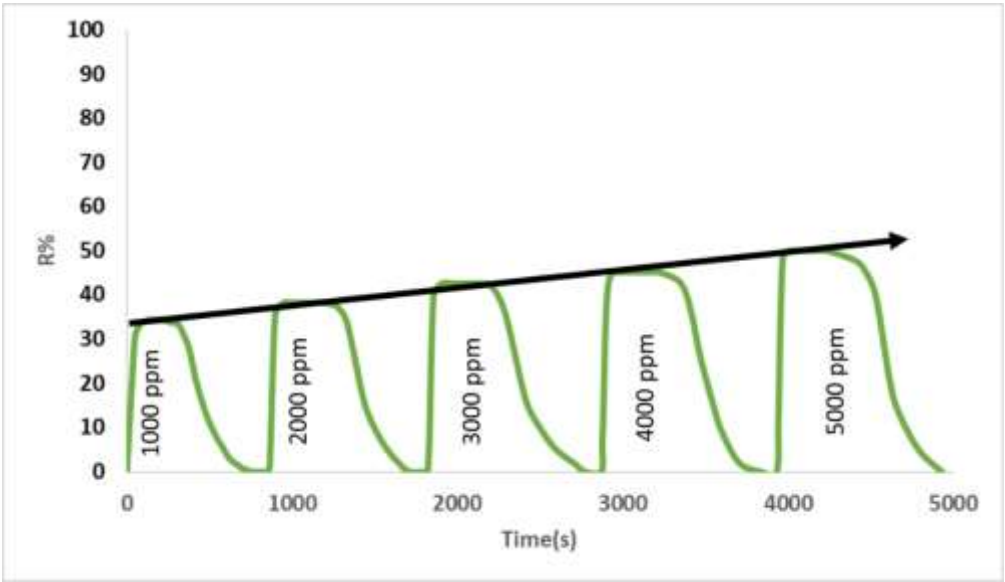

Figure 47: Combined Response curve of rGO/CoOOH Sensor

4.4.4. Response of rGO/ZIF-67

Figure 48 to 50 illustrates the sensing characteristics of rGO/ZIF-67. The response of rGO/ZIF-67 towards 1000ppm of CO level is shown in figure 48. As compare to the response of other sensors rGO/ZIF-67 have less response time and high sensitivity.

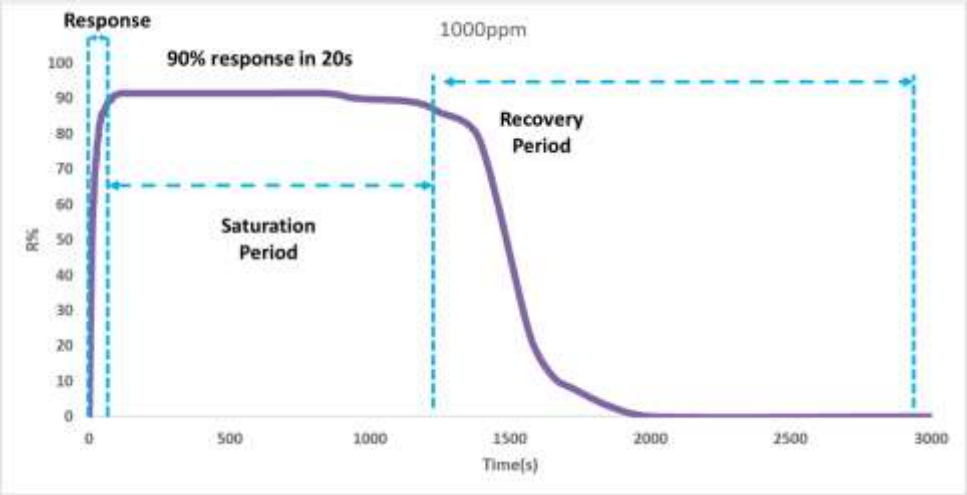

Figure 48: Dynamic Response Curve of rGO/ZIF-67 Sensor for 1000ppm of CO Level

Sensor show p-type sensing characteristics with of 91% at 1000ppm, 93% at 2000ppm, 95% at 3000ppm, 97% at 4000ppm and 98% sensitivity against 5000 ppm of CO exposure. As all of the dynamic response curves show, sensor response rises with the escalation of CO gas level and reach to saturation plateau after saturation curves move to desorption mode.

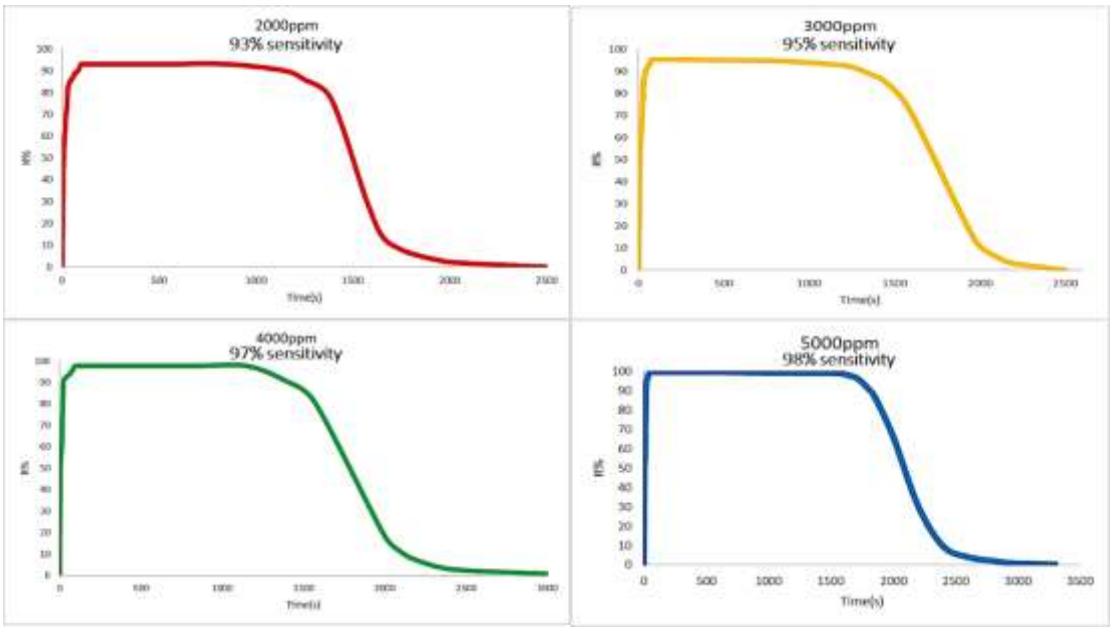

Figure 49: Dynamic Response Curves at Different CO Levels for rGO/ZIF-67 Sensor

The high response of rGO/ZIF-67 is because of high porosity and active Cobalt metal of ZIF-67. In ZIF-67 the oxidation state of Coblat is +3 and Cobalt +3 oxidation is very active towards CO oxidation. By combining all the response curves as shown in figure 50 as we can see that the percentage response increase with the increase in CO level but in case of rGO/ZIF-67 sensor this change is small.

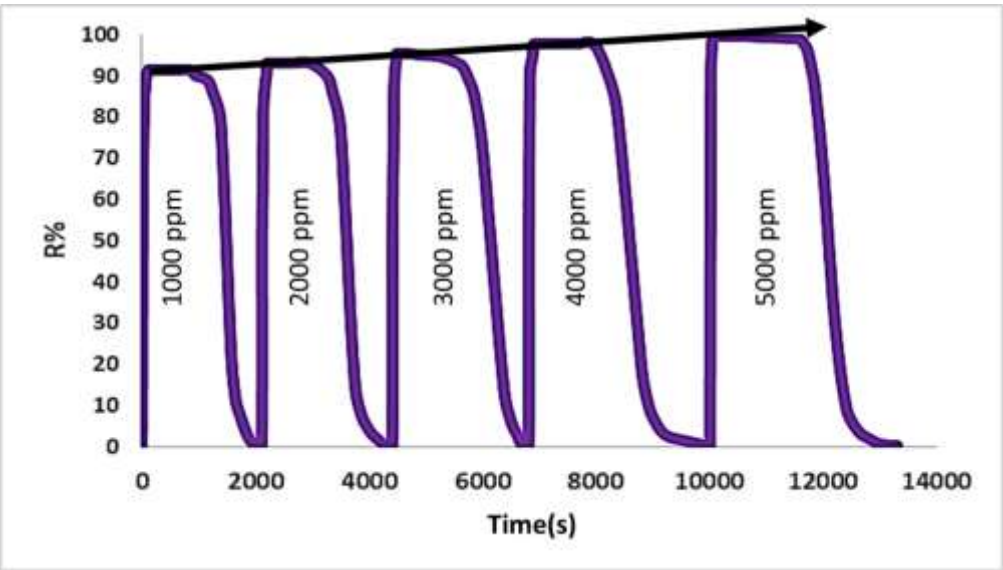

Figure 50: Combined Response curve of rGO/ZIF-67 Sensor

4.4.5. Response of rGO/Ni-BDC

Figure 51 to 53 illustrate the sensing characteristics of rGO/Ni-BDC. rGO/Ni-BDC sensor show only 35% response towards 1000ppm of CO level which is quite low as compare ZIF-67.

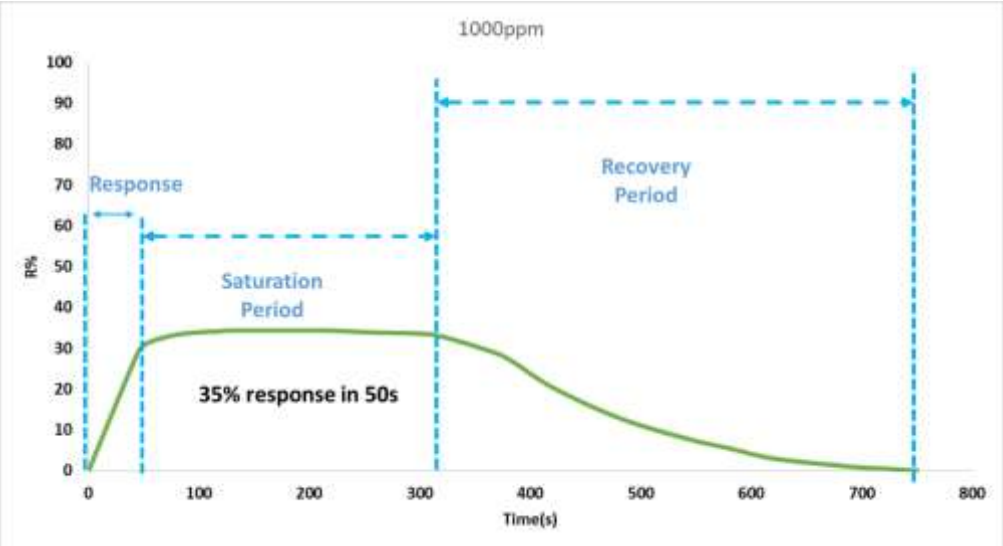

Figure 51: Dynamic Response Curve of rGO/Ni-BDC Sensor for 1000ppm of CO Level

Sensor show p-type sensing characteristics with 35 at 1000ppm, 44% at 2000ppm, 47% at 3000ppm, 49% at 4000ppm and 52% sensitivity against 5000 ppm of CO exposure at room temperature (30^{o}C) and average response time of 60s. The response is lower than rGO/ZIF-67 because Ni in +3 oxidation is not very active towards CO oxidation as compared to Co in +3 oxidation state.

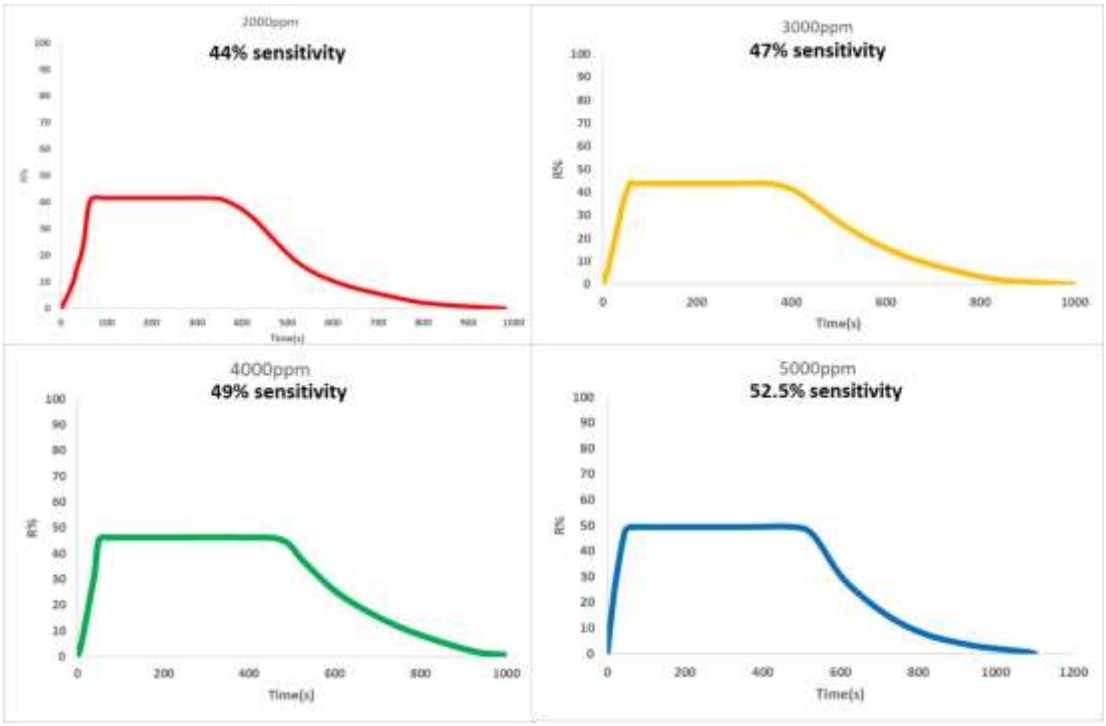

Figure 52: Dynamic Response Curves at Different CO Levels for rGO/Ni-BDC Sensor

As all of the dynamic response curves shows, sensor response rises with the escalation of CO gas concentration and reach to saturation plateau after saturation curves move to desorption mode which represent the recovery of sensor.

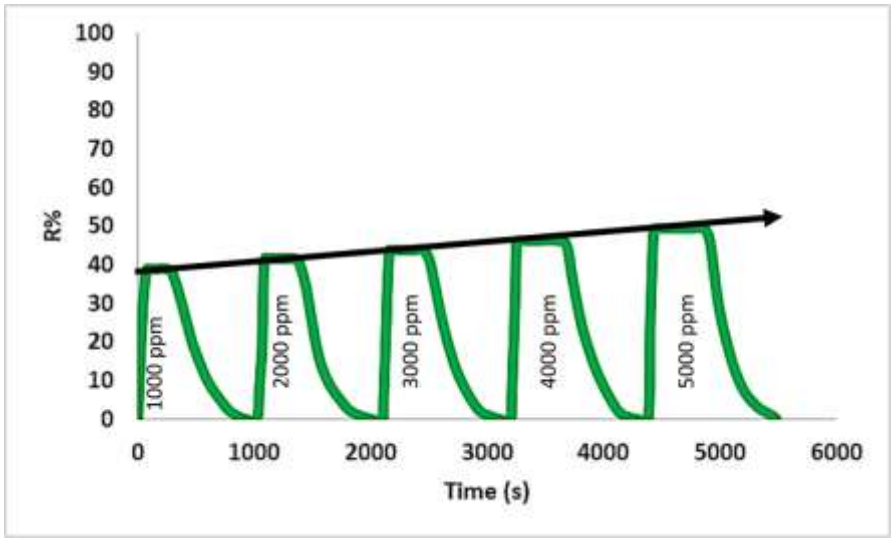

Figure 53: Combined Response curve of rGO/Ni-BDC Sensor

Summarized result of all the sensors is given in table 4.1 and 4.2.

Table 4.1: Summary of Response of Sensors

Material	**Response %**				
CO Levels	**1000 ppm**	**2000 ppm**	**3000 ppm**	**4000 ppm**	**5000 ppm**
Graphene					
rGO	-	-	-	-	14%
N-doped rGO	86%	89.6%	93%	96%	98%
rGO/Metal Oxides					
rGO/Fe_3O_4	No Response at Room Temperature				
rGO/CoOOH	35%	38%	42%	45%	49%
rGO/MOFs					
rGO/ZIF-67	91%	93%	95%	97%	98%
rGO/Ni-BDC	41%	44%	47%	49%	52.5%

Table 4.2: Response Time of Sensors

Material	**Time (sec)**
rGO	120s
N-rGO	30s
rGO/Fe_3O_4	No Response at Room Temperature
rGO/CoOOH	50s
rGO/ZIF-67	20s
rGO/Ni-BDC	60s

Conclusions

In this work, reduced graphene oxide and its derivate are studied for CO sensing application. CO sensing was carried out by using a chemi-resistive gas sensor. The sensor was tested for 1000ppm to 5000pm of CO level with an increment of 1000ppm value. Sensing study of sensors was performed by using a lab build setup. The sensor response of rGO synthesized by using modified Hummer's method was investigated for CO chemi-resistors gas sensor, the sensor showed inappreciable current variation of about 14% response upon CO exposure of 5000ppm. The reduced graphene oxide was made sensitive to CO by nitrogen doping in rGO sheets and making rGO composites with nanoparticles of metal oxide (Fe_3O_4 and CoOOH) and MOFs (ZIF-67 and Ni-BDC). Nitrogen doped rGO and rGO composites showed promising results compared to pristine rGO for CO sensing. The N-doped graphene effectively enhanced the CO sensing properties of rGO to 86% sensitivity for 1000ppm of CO level. Metal oxide rGO/CoOOH composite gives 35% response in 50s for 1000ppm of CO level at room temperature, while rGO/Fe_3O_4 gives no response for CO sensing at room temperature. Among two prepared composites of MOFs, Ni-BDC MOF gives 41% response in 60s for 1000ppm of CO level, while ZIF-67 gives highest sensitivity of 90% in 20s for 1000ppm of CO level. Overall, the prepared sensors showed response in ppm range while operating at ambient conditions. Upon combining metal oxide with rGO, the room temperature CO sensitivity can be enhanced. ZIF-67 and Ni-BDC metal organic frameworks based composites are potential candidates for CO chemi-resistive gas sensors.

Future Recommendations

- Graphene composites with MOFs can be studied for other gas sensors such as NH_3, CH_4, H_2S.
- Copper and Zinc based metal organic frameworks can be studied for CO sensing.
- Effect of temperature on CO sensing can be studied.
- Selectivity study of sensors towards CO can be studied in future work.

References

[1] J. Davies, “Hazardous Gas Model Evaluation with Field Observations.” *Atmospheric Environment*, vol. 29, no. 3, **1995**, pp. 456–457.

[2] J. Chou, Hazardous Gas Monitors: a Practical Guide to Selection, Operation and Applications. *McGraw-Hill*, **2001**.

[3] Air quality criteria for carbon monoxide. WHO Regional Office for Europe, Copenhagen, Denmark, **2000**. www.euro.who.int/__data/assets/pdf_file/.../AQG2ndEd_5_5carbonmonoxide.PDF

[4] UNITED STATES DEPARTMENT OF LABOR. (n.d.). Retrieved from https://www.osha.gov/Publications/OSHA3252/3252.html OSHA 3252-05N **2005**

[5] C. J. Johnson,, J. C. Moran, S. C. Paine, H. W. Anderson, and P. A. Breysse. “Abatement of Toxic Levels of Carbon Monoxide in Seattle Ice-Skating Rinks.” *American Journal of Public Health*, vol. 65, no. 10, **1975**, pp. 1087–1090.

[6] B. Marc, “Carbon-Monoxide Poisoning in Young Drug Addicts Due to Indoor Use of a Gasoline-Powered Generator.” *Journal of Clinical Forensic Medicine*, vol. 8, no. 2, **2001**, pp. 54–56.

[7] C. E. Fife, “Dying to Play Video Games: Carbon Monoxide Poisoning From Electrical Generators Used After Hurricane Ike.” *Pediatrics*, vol. 123, no. 6, **2009**,

[8] Olding, R. (2015, July 18). Man died from carbon monoxide poisoning after using 'heat beads' in Greystanes home. *The Sydney Morning Herald*. Retrieved September 14, **2018**, from https://www.smh.com.au/national/nsw/man-died-from-carbon-monoxide-poisoning-after-using-heat-beads-in-greystanes-home-20150718-gif8d8.html

[9] G. Korotcenkov, “Metal Oxides for Solid-State Gas Sensors: What Determines Our Choice?” *Materials Science and Engineering: B*, vol. 139, no. 1, **2007**, pp. 1–23.

[10] I. Eisele, T. Doll, M. Burgmair, “Low Power Gas Detection with FET Sensors.” *Sensors and Actuators B: Chemical*, vol. 78, no. 1-3, **2001**, pp. 19–25.

[11] G. Korotcenkov, “Gas Response Control through Structural and Chemical Modification of Metal Oxide Films: State of the Art and Approaches.” *Sensors and Actuators B: Chemical*, vol. 107, no. 1, **2005**, pp. 209–232.

[12] Noboru. Yamazoe, “Toward Innovations of Gas Sensor Technology.” *Sensors and Actuators B: Chemical*, vol. 108, no. 1-2, **200**5, pp. 2–14.

[13] V.v. Malyshev, and A.v. Pislyakov. “Investigation of Gas-Sensitivity of Sensor Structures to Hydrogen in a Wide Range of Temperature, Concentration and Humidity of Gas Medium.” *Sensors and Actuators B: Chemical*, vol. 134, no. 2, **2008**, pp. 913–921.

[14] M. Congcong. “Nitrogen-Doped Graphene as an Excellent Candidate for Selective Gas Sensing.” *Science China Chemistry*, vol. 57, no. 6, **2014**, pp. 911–917.

[15] A. K. Geim, and K. S. Novoselov. “The Rise of Graphene.” *Nature Materials*, vol. 6, no. 3, **2007**, pp. 183–191.

[16] L.Navarro, M. Pardo, N. Fabiola, et al. “Graphene/Polymer Nanocomposites: Crystal Structure, Mechanical and Thermal Properties.” *Graphene Science Handbook*, **2016**, pp. 77–98.

[17] B. C. Brodie, “On the Atomic Weight of Graphite.” *Proceedings of the Royal Society of London*, vol. 10, **1859**, pp. 11–12.

[18] W. Hummers, S. William, and E. Offeman. “Preparation of Graphitic Oxide.” *Journal of the American Chemical Society*, vol. 80, no. 6, **1958**, pp. 1339–1339.

[19] G.Ruess and F.Vogt. High-lamellar graphite oxide. ”*Monatsh. Chem.*” vol.78, no. 3, **1948**, pp.222–242.

[20] H. Boehm, R. Setton, and E. Stumpp. Nomenclature and terminology of graphite intercalation compounds. *Carbon*, vol.24, no.2, **1986**, pp. 241–245.

[21] K. S. Novos¨elov, A. K. Geim, S. V. Morozov, D. Jiang, Y. Zhang, S. V. Dubonos, I. V. Grigorieva, and A. A. Firsov. Electric Field Effect in Atomically Thin Carbon Films. *Science*, vol.306, no.5696, **2004**, pp. 666–669.

[22] Park, Hye Jin, et al. “Growth and Properties of Few-Layer Graphene Prepared by Chemical Vapor Deposition.” *Carbon*, vol. 48, no. 4, **2010**, pp. 1088–1094.

[23] V. Emtsev, Konstantin. “Towards Wafer-Size Graphene Layers by Atmospheric Pressure Graphitization of Silicon Carbide.” *Nature Materials*, vol. 8, no. 3, **2009**, pp. 203–207.

[24] Adrian Balan,. “Anodic Bonded Graphene.” *Journal of Physics D: Applied Physics*, vol. 43, no. 37, **2010**, p. 374013.

[25] L. Hernandez and W. Yenny, “High-Yield Production of Graphene by Liquid-Phase Exfoliation of Graphite,” *Nature Nanotechnology*, vol. 3, no. 9, **2008**, pp. 563–568.

[26] X. Wang, L. Zhi, K. Mullen, “Transparent, conductive graphene electrodes for dye-sensitized solar cells,” *Nano Letter*, vol. 8, no.1, **2008**, pp.323–7.

[27] Z. Wu, S. Ren, W.Gao, J.Zhao, Z. Chen, B. Liu, et al. “Synthesis of graphene sheets with high electrical conductivity and good thermal stablility by hydrogen arc discharge exfoliation.” *ACS Nano*, vol.3, no. 2, **2009**, pp.411–7.

[28] X. Li, H. Wang, T. Robinson, H. Sanchez and H. Dai, “Simultaneous nitrogen doping and reduction of graphene oxide, *Journal of the American Chemical Society*” vol. 131, no. 43, **2009**, pp. 15939–44.

[29] Y. Zhu, S. Murali, MD. Stoller and A. Velamakanni, “Microwave assisted exfoliation and reduction of graphite oxide for ultracapacitors.” *Carbon*, vol. 48,no.7, **2010**, pp. 2118–22.

[30] LJ. Cote, R. Silva, J. Huang, “Flash reduction and patterning of graphite oxide and its polymer composite.” *Journal of the American Chemical Society*, vol. 131, no. 31, pp. 11027–32.

[31] Y. Zhang, L. Guo, S. Wei, Y. He and H. Xia, ”Direct imprinting of microcircuits on graphene oxides film by femtosecond laser reduction,” *Nanotoday*, vol. 5, no. 1, **2010**, pp. 15–20.

[32] G. Williams, B. Seger, PV. Kamat, “TiO_2-graphene nanocomposites. UV-assisted photocatalytic reduction of graphene oxide,” *ACS Nano* vol.2, no. 7, pp. 1487–91.

[33] Y. Iwase, A. Kudo and R. Amal, “Reducing graphene oxide on a visible-light bivo4 photocatalyst for an enhanced photoelectrochemical water splitting,” *Journal of Physical Chemistry Letters*, vol. 1, no.17, **2010**, pp. 2607–12.

[34] G. Williams and PV. Kamat, “Graphene semiconductor nanocomposites: excited-state interactions between ZnO nanoparticles and graphene oxide,” *Langmuir*, vol. 25, no. 24, **2009**, pp.13869–73.

[35] GK. Ramesha and S. Sampath, ‘Electrochemical reduction of oriented graphene oxide films: an in situ raman spectroelectrochemical study,” *Journal of Physical Chemistry Letters*, vol.113, no. 19, **2009**, pp.7985–9.

[36] S. Stankovich, DA. Dikin, RD. Piner, KA. Kohlhaas, A. Kleinhammes and Y. Jia, “Synthesis of graphene-based nanosheets via chemical reduction of exfoliated graphite oxide,” *Carbon*, vol. 45, no. 7, **2007**, pp. 1558–65.

[37] S. Pei, J. Zhao, J. Du, W. Ren and M. Cheng, “Direct reduction of graphene oxide films into highly conductive and flexible graphene films by hydrohalic acids,” *Carbon*, vol. 48, no. 15, 2010, pp. 4466–74.

[38] H. Shin, KK. Kim, A. Benayad, S. Yoon and HK. Park, “Efficient reduction of graphite oxide by sodium borohydride and its effect on electrical conductance,” *Advanced Functional Materials*, vol.19, no. 12, **2009**, pp. 1987–92.

[39] K. Moon, J. Lee, RS. Ruoff and H. Lee, “Reduced graphene oxide by chemical graphitization,” *Nature Communications*, vol. 1, no. 1, **2010**, pp. 73–8.

[40] Stankovich S, Dikin DA and Piner RD, “Synthesis of graphene-based nanosheets via chemical reduction of exfoliated graphite oxide,” *Carbon*, vol. 45, no. 7, **2007**, pp. 1558–65.

[41] J .Fernandez, L. Guardia, JI. Paredes and S. Villar, “Vitamin C is an ideal substitute for hydrazine in the reduction of graphene oxide suspensions,” *Journal of Physical Chemistry Letters*, vol. 114, no. 14, **2010**, pp. 6426–32.

[42] Y. Zhou, Q. Bao and KP. Loh, “Hydrothermal dehydration for the ‘‘green’’ reduction of exfoliated graphene oxide to graphene and demonstration of tunable optical limiting properties,” *Chemistry of Materials*, vol. 21, no. 13, **2009**, pp. 2950–6.

[43] H. Wang, JT. Robinson, X. Li and H. Dai, “Solvothermal reduction of chemically exfoliated graphene sheets,” *Journal of the American Chemical Society*, vol. 131, no. 29, **2009**, pp. 9910–1.

[44] S. Dubin, S. Gilje, K. Wang and AS. Hall, “A one-step solvothermal reduction method for producing reduced graphene oxide dispersions in organic solvents,” *ACS Nano*, vol. 4, no. 7, **2010**, pp. 3845–52

[45] W. Gao, LB. Alemany and L. Ajayan, “New insights into the structure and reduction of graphite oxide,” *Nature Communications*, vol. 1, no. 5, **2009**, pp. 403–8.

[46] HA. Becerril, J. Mao, and Y. Chen, “Evaluation of solution-processed reduced graphene oxide films as transparent conductors,” *ACS Nano*, vol. 2, no. 3, 2008, pp. 463–70.

[47] C. Lijie,“Atomic Layers of Hybridized Boron Nitride and Graphene Domains.” *Nature Materials*, vol. 9, no. 5, **2010**, pp. 430–435.

[48] J. Kotakoski, A. Krasheninnikov, K. Nordlund, R. M. Nieminen, “B and N Ion Implantation into Carbon Nanotubes: Insight from Atomistic Simulations.” *Physical Review B*, vol. 71, no. 20, **2005**.

[49] T. B. Martins, “Electronic and Transport Properties of Boron-Doped Graphene Nanoribbons.” *Physical Review Letters*, vol. 98, no. 19, **2007**, pp.11

[50] Pablo Denis, “Band Gap Opening of Monolayer and Bilayer Graphene Doped with Aluminium, Silicon, Phosphorus, and Sulfur.” *Chemical Physics Letters*, vol. 492, no. 4-6, **2010**, pp. 251–257.

[51] Aktürk, Olcay Üzengi, and Mehmet Tomak. “Bismuth Doping of Graphene.” *Applied Physics Letters*, vol. 96, no. 8, **2010**, p. 081914.

[52] Dacheng Wei, “Synthesis of N-Doped Graphene by Chemical Vapor Deposition and Its Electrical Properties.” *Nano Letters*, vol. 9, no. 5, **2009**, pp. 1752–1758.

[53] M. Li, W. Zhongshuai, R. Wencai “The Doping of Reduced Graphene Oxide with Nitrogen and Its Effect on the Quenching of the Material’s Photoluminescence.” *Carbon*, vol. 50, no. 14, **2012**, pp. 5286–5291.

[54] F. Xiaogang, “FeCo–Nx Embedded Graphene as High Performance Catalysts for Oxygen Reduction Reaction.” *Applied Catalysis B: Environmental*, vol. 130-131, **2013**, pp. 143–151.

[55] L. Guan, “Preparation of Few-Layer Nitrogen-Doped Graphene Nanosheets by DC Arc Discharge under Nitrogen Atmosphere of High Temperature.” *Applied Physics A*, vol. 102, no. 2, **2010**, pp. 289–294.

[56] H. Wang and Z. Ying, “Nitrogen-Doped Graphene and Its Application in Electrochemical Biosensing.” *ACS Nano*, vol. 4, no. 4, **2010**, pp. 1790–1798.

[57] W. Hwang, K. Jin, "Workfunction-Tunable, N-Doped Reduced Graphene Transparent Electrodes for High-Performance Polymer Light-Emitting Diodes." *ACS Nano*, vol. 6, no. 1, **2011**, pp. 159–167.

[58] W. Jiang and J. Baojiang, "Highly Concentrated, Stable Nitrogen-Doped Graphene for Supercapacitors: Simultaneous Doping and Reduction." *Applied Surface Science*, vol. 258, no. 8, **2012**, pp. 3438–3443.

[59] Jincheng Bai, Qianqian Zhu, Zhexin Lv, Hongzhou Dong, Jianhua Yu and Lifeng Dong "Nitrogen-Doped Graphene as Catalysts and Catalyst Supports for Oxygen Reduction in Both Acidic and Alkaline Solutions." International *Journal of Hydrogen Energy*, vol. 38, no. 3, **2013**, pp. 1413–1418.

[60] Zhang, Yuanjian, "Wet Chemical Synthesis of Nitrogen-Doped Graphene towards Oxygen Reduction Electrocatalysts without High-Temperature Pyrolysis." *Journal of Materials Chemistry*, vol. 22, no. 14, **2012**, p. 6575

[61] Wang, Xianlong, "Theoretical Characterization of X-Ray Absorption, Emission, and Photoelectron Spectra of Nitrogen Doped along Graphene Edges." *The Journal of Physical Chemistry A*, vol. 117, no. 3, **2013**, pp. 579–589.

[62] C. P. Ewels, and M. Glerup. "Nitrogen Doping in Carbon Nanotubes." *Journal of Nanoscience and Nanotechnology*, vol. 5, no. 9, **2005**, pp. 1345–1363.

[63] V. Casanovas, J. Jordi, "Origin of the Large N 1s Binding Energy in X-Ray Photoelectron Spectra of Calcined Carbonaceous Materials." *Journal of the American Chemical Society*, vol. 118, no. 34, **1996**, pp. 8071–8076.

[64] Brattain, H. Walter, and John Bardeen, "Surface Properties of Germanium." *Bell System Technical Journal*, vol. 32, no. 1, **1953**, pp. 1–41.

[65] Yamazoe Noboru. "New Approaches for Improving Semiconductor Gas Sensors." *Sensors and Actuators B: Chemical*, vol. 5, no. 1-4, **1991**, pp. 7–19.

[66] G. Kiriakidis, H. Ouacha and N. Katsarakis "Growth and Gas-Sensing Studies of Metal Oxide Semiconductor Nanostructures." *International Journal of Nanotechnology*, vol. 7, no. 9, **2010**, pp. 883.

[67] Shanmugasundaram, Arunkumar, "Realizing Synergy between In_2O_3 Nanocubes and Nitrogen-Doped Reduced Graphene Oxide: An Excellent Nanocomposite for the Selective and Sensitive Detection of CO at Ambient Temperatures." *ACS Applied Materials & Interfaces*, vol. 9, no. 37, **2017**, pp. 31728–31740.

[68] O. K. Farha, C. E. Wilmer, I. Eryazici, B. G. Hauser, P. A. Parilla and K. O'Neill, "Designing higher surface area metal–organic frameworks: are triple bonds better than phenyls?," *Journal of the American Chemical Society*, vol. 134, **2012**, pp. 9860-9863.

[69] B. Chen, C. Liang, J. Yang, D. S. Contreras, Y. L. Clancy and E. B. Lobkovsky, "A Microporous Metal–Organic Framework for Gas-Chromatographic Separation of Alkanes," *Angewandte Chemie*, vol. 118, **2006**, pp. 1418-1421.

[70] K. S. Walton and R. Q. Snurr, "Applicability of the BET method for determining surface areas of microporous metal−organic frameworks," *Journal of the American Chemical Society*, vol. 129, **2007**, pp. 8552-8556.

[71] J. Ren, X. Dyosiba, N. M. Musyoka, H. W. Langmi, M. Mathe, and S. Liao, "Review on the current practices and efforts towards pilot-scale production of metal-organic frameworks (MOFs)," *Coordination Chemistry Reviews*, vol. 352, **2017**, pp. 187-219.

[72] G. Férey, "Hybrid porous solids: past, present, future," *Chemical Society Reviews*, vol. 37, **2008**, pp. 191-214.

[73] W. Ren and J. Jang, et al. "Use of Cobalt Oxide CoOOH in a Carbon Monoxide Sensor Operating at Low Temperatures." *Sensors and Actuators B: Chemical*, vol. 120, no. 1, **2006**, pp. 104–109.

[74] Fazel Yavari, Eduardo Castillo and Hemtej Gullapalli, "High Sensitivity Detection of NO_2 and NH_3 in Air Using Chemical Vapor Deposition Grown Graphene." *Applied Physics Letters*, vol. 100, no. 20, **2012**, p. 203120.

[75] Lei Huang, "Fully Printed, Rapid-Response Sensors Based on Chemically Modified Graphene for Detecting NO_2 at Room Temperature." *ACS Applied Materials & Interfaces*, vol. 6, no. 10, **2014**, pp. 7426–7433.

[76] K. R.. Nemade and S. A. Waghuley, "Carbon Dioxide Gas Sensing Application Of Graphene/Y_2O_3 Quantum Dots Composite." *International Journal of Modern Physics: Conference Series*, vol. 22, **2013**, pp. 380–384.

[77] (a) K.r. Nemade,, and S.a. Waghuley. "Role of Defects Concentration on Optical and Carbon Dioxide Gas Sensing Properties of Sb_2O_3/Graphene Composites." *Optical Materials*, vol. 36, no. 3, **2014**, pp. 712–716.

[78] Johnson and L. Jason “Hydrogen Sensing Using Pd-Functionalized Multi-Layer Graphene Nanoribbon Networks.” *Advanced Materials*, vol. 22, no. 43, **2010**, pp. 4877–4880.

[79] W. Zuquan, X. Chen, S. Zhu “Room Temperature Methane Sensor Based on Graphene Nanosheets/Polyaniline Nanocomposite Thin Film.” *IEEE Sensors Journal*, vol. 13, no. 2, **2013**, pp. 777–782.

[80] L. Tang, H. Longhua, “Uniform and Rich-Wrinkled Electrophoretic Deposited Graphene Film: a Robust Electrochemical Platform for TNT Sensing.” *Chemical Communications*, vol. 46, no. 32, **2010**, p. 5882.

[81] L. Zhou, F. Shen, X. Tian, “Stable Cu_2O Nanocrystals Grown on Functionalized Graphene Sheets and Room Temperature H_2S Gas Sensing with Ultrahigh Sensitivity.” *Nanoscale*, vol. 5, no. 4, **2013**, p. 1564.

[82] W. Yadav, E. Roshni, and C.k. Dixit. “Synthesis, Characterization and Prospective Applications of Nitrogen-Doped Graphene: A Short Review.” *Journal of Science: Advanced Materials and Devices*, vol. 2, no. 2, **2017**, pp. 141–149.,

[83] Ma. Congcong, “Nitrogen-Doped Graphene as an Excellent Candidate for Selective Gas Sensing.” *Science China Chemistry*, vol. 57, no. 6, **2014**, pp. 911–917.

[84] T. Hübert, “Hydrogen Sensors – A Review.” *Sensors and Actuators B: Chemical*, vol. 157, no. 2, **2011**, pp. 329–352.

[85] P. Nag, S. Majumdar, A. Bumajdad, P. Devi, “Enhanced Gas Sensing Performance of Tin Dioxide- Based Nanoparticles for a Wide Range of Concentrations of Hydrogen Gas.” *RSC Advances*, vol. 4, no. 36, **2014**, p. 18512.

[86] L. Boon and J. Brett, “Identifying Performance Gaps in Hydrogen Safety Sensor Technology for Automotive and Stationary Applications.” *International Journal of Hydrogen Energy*, vol. 35, no. 1, **2010**, pp. 373–384.

[87] M. Shojaee, “Hydrothermally Synthesized Pd-Loaded SnO_2/Partially Reduced Graphene Oxide Nanocomposite for Effective Detection of Carbon Monoxide at Room Temperature.” *Sensors and Actuators B: Chemical*, vol. 254, **2018**, pp. 457–467.

[88] D. Zhang, Y. Sun, C. Jianga and Y. Zhang, "Room-Temperature Highly Sensitive CO Gas Sensor Based on Ag-Loaded Zinc Oxide/Molybdenum Disulfide Ternary Nanocomposite and Its Sensing Properties." *Sensors and Actuators B: Chemical*, vol. 253, **2017**, pp. 1120–1128.

[89] B. Kim and J. Beomseok, et al. "Low Temperature Pd/SnO_2 Sensor for Carbon Monoxide Detection." *Sensors and Actuators B: Chemical*, vol. 177, **2013**, pp. 770–775.

[90] F. Huifen, H. Changliang and W. Zhihua, "Facile Preparation of Rod-like Au/In_2O_3 Nanocomposites Exhibiting High Response to CO at Room Temperature." *Sensors and Actuators B: Chemical*, vol. 243, **2017**, pp. 516–524.

[91] J.f. Chang, "The Effects of Thickness and Operation Temperature on ZnO:Al Thin Film CO Gas Sensor." *Sensors and Actuators B: Chemical*, vol. 84, no. 2-3, **2002**, pp. 258–264.

[92] Y. Haeng, and G. Choi. "Selective CO Gas Detection of CuO- and ZnO-Doped SnO_2 Gas Sensor." *Sensors and Actuators B: Chemical*, vol. 75, no. 1-2, **2001**, pp. 56–61.

[93] W. Ren, "Use of Cobalt Oxide CoOOH in a Carbon Monoxide Sensor Operating at Low Temperatures." *Sensors and Actuators B: Chemical*, vol. 120, no. 1, **2006**, pp. 104–109.

[94] L. Hsiang, and H. Chen, "Highly Sensitive Room-Temperature CO Gas Sensors: Pt and Pd Nanoparticle-Decorated In_2O_3 Flower-like Nanobundles." *Journal of Materials Chemistry*, vol. 22, no. 26, **2012**, pp. 13204.

[95] W. Ning, D. Hui, Z. Xiangyang and M.Yang "Homogeneous Coating of Au and SnO_2 Nanocrystals on Carbon Nanotubes via Layer-by-Layer Assembly: a New Ternary Hybrid for a Room-Temperature CO Gas Sensor." *Chemical Communications*, no. 46, **2008**, p. 6182.

[96] S. Arunkumar, "Au Decorated ZnO Hierarchical Architectures: Facile Synthesis, Tunable Morphology and Enhanced CO Detection at Room Temperature." *Sensors and Actuators B: Chemical*, vol. 243, **2017**, pp. 990–1001.

[97] J. Kim and A. Katoch "Realization of Ppm-Level CO Detection with Exceptionally High Sensitivity Using Reduced Graphene Oxide-Loaded SnO_2

Nanofibers with Simultaneous Au Functionalization." *Chemical Communications*, vol. 52, no. 19, **2016**, pp. 3832–3835.

[98] N. Kumar, A. Srivastava and H. Patel, "Enhanced Gas Sensing Properties to Acetone Vapor Achieved by α-Fe_2O_3 Particles Ameliorated with Reduced Graphene Oxide Sheets." *Sensors and Actuators B: Chemical*, vol. 241, **2017**, pp. 904–914.

[99] N. Kumar and H. Nagesh, "Facile Synthesis of ZnO-Reduced Graphene Oxide Nanocomposites for NO_2 Gas Sensing Applications." *European Journal of Inorganic Chemistry*, vol. 2015, no. 11, **2015**, pp. 1912–1923.

[100] W. Yang, Y. Wei, "Additive-Free Synthesis of In_2O_3 Cubes Embedded into Graphene Sheets and Their Enhanced NO_2 Sensing Performance at Room Temperature." *ACS Applied Materials & Interfaces*, vol. 6, no. 23, **2014**, pp. 21093–21100.

[101] J. Peng, and C.Chai, "A Study of the Sensing Characteristics of Fe_2O_3 Gas-Sensing Thin Film." *Sensors and Actuators B: Chemical*, vol. 14, no. 1-3, **1993**, pp. 591–593.

[102] G. S. Korotchenkov, Handbook of Gas Sensor Materials: Properties, Advantages and Shortcomings for Applications. *Springer*, **2013**.

[103] Q. Lee, J. Heun, "Gas Sensors Using Hierarchical and Hollow Oxide Nanostructures: Overview." *Sensors and Actuators B: Chemical*, vol. 140, no. 1, **2009**, pp. 319–336.

[104] L. Xiaomei, G. Gongmin, L. Zheng, "Encapsulation of Strongly Fluorescent Carbon Quantum Dots in Metal–Organic Frameworks for Enhancing Chemical Sensing." *Analytical Chemistry*, vol. 86, no. 2, **2013**, pp. 1223–1228.

[105] Cao, Xiehong, et al. "Metal Oxide-Coated Three-Dimensional Graphene Prepared by the Use of Metal-Organic Frameworks as Precursors." *Angewandte Chemie*, vol. 126, no. 5, **2013**, pp. 1428–1433.

[106] C. Xiehong, B. Zheng, X. Rui, W.Shi and H. Zhang, "The Application of ZIF-67 and Its Derivatives: Adsorption, Separation, Electrochemistry and Catalysts." *Journal of Materials Chemistry A*, vol. 6, no. 5, **2018**, pp. 1887–1899.

[107] J. Wenlan, "Metal–Organic Framework Derivatives for Improving the Catalytic Activity of the CO Oxidation Reaction." *ACS Applied Materials & Interfaces*, vol. 9, no. 18, **2017**, pp. 15394–15398.

[108] K. S. Park, Z. Ni, A. P. Côté, J. Y. Choi, R. Huang and F. J. Uribe, "Exceptional chemical and thermal stability of zeolitic imidazolate frameworks," *Proceedings of the National Academy of Sciences*, vol. 103, **2006**, pp. 10186-10191.

[109] S.Gao, Y.Sui, F.Wei, J.Qi, "Facile Synthesis of Cuboid Ni-MOF for High-Performance Supercapacitors." *Journal of Materials Science*, vol. 53, no. 9, Dec. **2018**, pp. 6807–6818.

[110] W. Hummers and R. Offeman. "Preparation of Graphitic Oxide." *Journal of the American Chemical Society*, vol. 80, no. 6, **1958**, pp. 1339– 1339.

[111] C. Marcano, "Improved Synthesis of Graphene Oxide." *ACS Nano*, vol. 4, no. 8, **2010**, pp. 4806–4814.

[112] J. Zhang, H.Yang and G. Shen, "Reduction of Graphene Oxide Vial-Ascorbic Acid." *Chemical Communications*, vol. 46, no. 7, **2010**, pp. 1112–1114.

[113] H. Sun, "Facile Synthesis of Nitrogen Doped Reduced Graphene Oxide as a Superior Metal-Free Catalyst for Oxidation." *Chemical Communications*, vol. 49, no. 85, **2013**, p. 9914.

[114] T. Jiao, Y. Liu, Y. Wu, Q. Zhang and X. Yan, "Facile and Scalable Preparation of Graphene Oxide-Based Magnetic Hybrids for Fast and Highly Efficient Removal of Organic Dyes." *Scientific Reports*, vol. 5, no. 1, **2015.**

[115] A. Hosseinian, "Nanocomposite of ZIF-67 Metal–Organic Framework with Reduced Graphene Oxide Nanosheets for High-Performance Supercapacitor Applications." *Journal of Materials Science: Materials in Electronics*, vol. 28, no. 23, **2017**, pp. 18040–18048

[116] S. Kaimin. X-Ray Diffraction Structure, Principles and Applications. Nova Publications, **2013**.

[117] J. Goodhew, et al. Electron Microscopy and Analysis. *Taylor & Francis*, **2001**.

[118] L. Smith and T. Brian, Fundamentals of Fourier Transform Infrared Spectroscopy. *CRC Press*, **2011**.

[119] L. Stobinski, B. Lesiak, A. Malolepszy and M. Mazurkiewiczet "Graphene Oxide and Reduced Graphene Oxide Studied by the XRD, TEM and Electron Spectroscopy Methods." *Journal of Electron Spectroscopy and Related Phenomena*, vol. 195, **2014**, pp. 145–154.

[120] K. Panchariya and K. Dharmendra,"Core–Shell Zeolitic Imidazolate Frameworks for Enhanced Hydrogen Storage." *ACS Omega*, vol. 3, no. 1, May **2018**, pp. 167–175.

[121] A. Jagadale, D. Dubal and C. Lokhande, "Electrochemical Behavior of Potentiodynamically Deposited Cobalt Oxyhydroxide (CoOOH) Thin Films for Supercapacitor Application." *Materials Research Bulletin*, vol. 47, no. 3, **2012**, pp. 672–676.